

## Deviatoric Elasticity as a Mechanism describing Stable Shapes of Nanotubes

Veronika Kralj-Iglič,<sup>1</sup> Maja Remškar,<sup>2</sup> and Aleš Iglič<sup>3</sup>  
1. Institute of Biophysics, Faculty of Medicine, Slovenia  
2. J. Stefan Institute, Slovenia  
3. Faculty of Electrical Engineering, Slovenia

Recently, attention is being devoted to structures of nanometer dimensions due to potential benefit in biology and technology.

Experiments show that elongated thin structures (nanotubes) exist in organic and in inorganic systems. Long thin organic structures were found to be composed of surfactants [1, 2, 3, 4, 5, 6], phospholipid membrane [7, 8, 9], erythrocyte membrane at special conditions [10, 11, 12, 13] and of cellular membranes [14, 15, 16]. In inorganic systems, the carbon nanotubes [17, 18, 19] have been hitherto given most attention [20], however, nanotubes composed of other materials such as boron nitride [21, 22], metal dichalcogenides [23, 24, 25, 26], TiO<sub>2</sub> [27, 28], GaN [29], Sb<sub>2</sub>O<sub>3</sub> and Sb<sub>2</sub>O<sub>5</sub> [30] and NbS<sub>2</sub> [31], have also been observed.

Fig.1 shows two examples of nanotubes: organic nanotubes that are obtained from erythrocyte membrane by adding a detergent dodecylmaltoside to the erythrocyte suspension and inorganic nanotube composed of MoS<sub>2</sub> obtained by chemical transport reaction at high temperature.

Besides potential benefit, nanotubes are also of interest as they represent frontiers with respect to physical tools. In such elongated thin structures granularity with respect to the constituting molecules or atoms becomes closer to the smallest extension of the entire structure so that in description of these systems, even qualitative validity of standard continuum approaches cannot be taken for granted.

In this contribution we present experiments on some organic and inorganic hollow nanotubes and follow their theoretical description starting from a single-constituent energy. Statistical mechanical methods are appropriate to describe the average behavior of the system constituents. The methods based on statistical mechanical approach lead to useful description only within the framework of afore chosen thermodynamic quantities that are reflected in measurements. The necessary thermodynamic framework is in our case provided by the elastic properties that are reflected in the shape of the nanotubes. It is demonstrated that the principles of deviatoric elasticity can be applied to organic and to inorganic nanotubes.

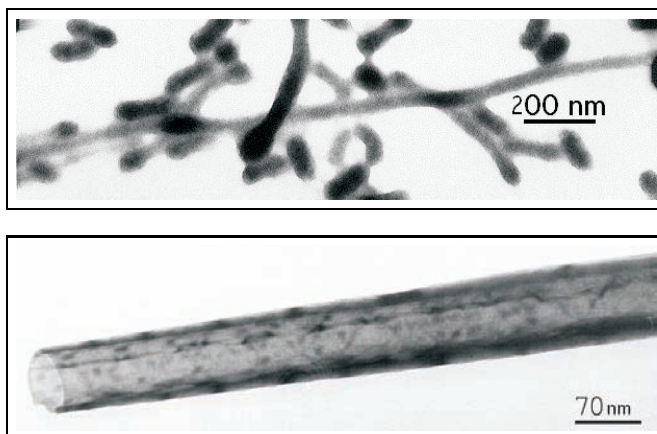


Figure 1: Upper picture: a transmission electron microscope image of the tubular nanoexovesicles released from the erythrocyte membrane. The erythrocyte suspension was incubated with a detergent dodecylmaltoside (which induced budding of the membrane) and then pelleted by centrifugation. A drop of therefrom isolated nanoexovesicles was applied on a formvar-coated grid. After drying, fixing and staining the nanoexovesicles were observed under Joel 100SX electron microscope ([32]). Lower picture: a transmission electron microscope image of the  $\text{MoS}_2$  nanotube grown by chemical transport reaction at 1010 K. The nanotube is hollow with open end. Its wall, 8 nm in thickness is composed of chirally grown S – Mo – S molecular layers ([33]).

## 1 The systems

In this section we will briefly describe the two systems forming the substance of the nanotubes that are the subject of our experimental study: phospholipid bilayer in the aqueous solution and a single  $\text{MoS}_2$  molecular layer composed of coaxial sulphur - molybdenum - sulphur cylinders.

### 1.1 Phospholipid bilayer

Phospholipid molecules can be described as composed of two parts: a multipolar headgroup and two carbohydrate  $(\text{CH}_2)_n - \text{CH}_3$  tails. The two tails may be of different lengths and may also contain double bonds between the carbon atoms (for a thorough description of different phospholipid molecules see for example an excellent book by Cevc and Marsh [34]). When mixed with water above a certain threshold concentration the phospholipid molecules assemble into a bilayer (Fig.2) so that the tails are hidden from the water. In this way the least of the hydrogen bonds between the water molecules are broken due to the presence of phospholipid molecules. Additionally, the phospholipid headgroups can interact with the adjacent water molecules. The thickness of the bilayer is around 5 nm [34]. It is

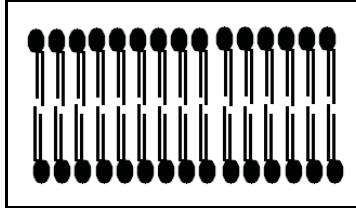


Figure 2: A scheme of a phospholipid bilayer. A phospholipid molecule is composed of a headgroup and two tails.

also energetically favorable that the bilayer closes upon itself to avoid the contact of hydrocarbon chains with water at the boundaries. Closing of the bilayer yields phospholipid bilayer vesicles. Various shapes and sizes of the vesicles were observed [35]. In simple systems composed of water solution and phospholipid, the shape of the phospholipid vesicle is determined by the properties of the phospholipid bilayer and by the external fields (if any). Therefore, the experiments where the shape can be observed in a controlled environment give important information on the physical mechanisms that are acting in the phospholipid bilayer membrane.

It is established that the phospholipid bilayer is an essential constitutive part of cellular membranes [36]. In this light phospholipid vesicles can be viewed as a convenient system where we expect to learn more about the function of the cellular membranes and ultimately, how to influence the function of the cell.

## 1.2 S – Mo – S molecular layer

The  $\text{MoS}_2$  compound belong to Group VI family of transition metal dichalcogenides with extremely non-isotropic layer type structure. The weak interaction holding the layers is in great part of van der Waals type. The single S-Mo-S molecular layer shows a trigonal symmetry (Fig.3a). The transition metal atom is co-ordinated by six sulphur atoms situated at corners of a trigonal prism. The molecular layers can be stacked in two ways, as a hexagonal polytype 2Hb (Fig. 3b) with two molecular layers (P63/mmc) and as rhombohedral polytype 3R (Fig. 3c) with three molecular layers per unit cell (R3m). At special conditions both polytypes can nucleate simultaneously [37].

In materials with low-dimensional structures, the instability of weakly bonded crystalline sheets against folding and the saturation of dangling bonds in self-terminated planes stabilize spherical or cylindrical crystal shapes in opposition to flat geometry. The nonalloyed nanotubes are always found in the helical forms [38, 23, 39]. Projection of a tube axis onto the basal  $[0001]$  plane of the wall is rotated with respect to the  $\langle 10\bar{1}0 \rangle$  lattice directions for an angle of chirality  $\alpha$ . Different chiralities were found in the nanotubes, from a few degrees up to  $20^\circ$ . Frequently, several chiralities are present even in a same nanotube, especially in the thick-walled nanotubes with diameters below 100 nm.

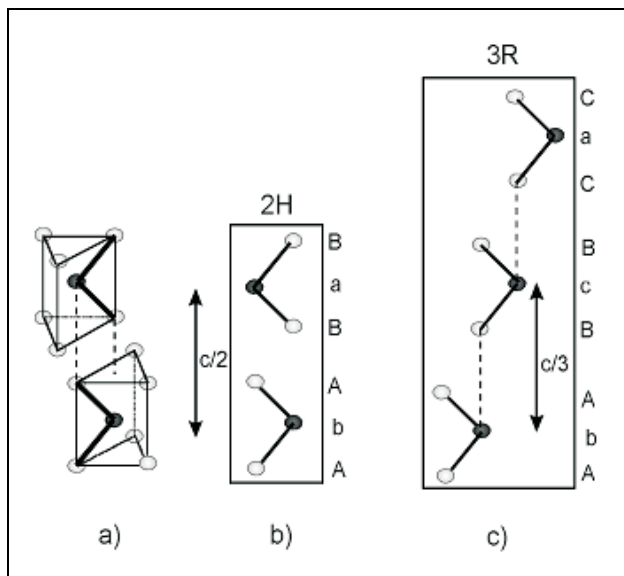


Figure 3: Two possible stacking of adjacent MoS<sub>2</sub> molecular layers: a) 3-dimensional model of the stable 2Hb stacking; b) and c) the [1120] sections of 2H and 3R stacking, respectively. Black circles represent Mo atoms while light circles represent S atoms.

The nanotubes' walls compose of different number of molecular layers, from two molecular layers in an extreme case up to several tens molecular layers in thick-walled nanotubes. Up to now, a single molecular layer MoS<sub>2</sub> nanotube with a diameter above 1 nm was not yet confirmed by experiment. Reducing the diameter, a new family of inorganic nanotubes appeared (assigned in the first report [26] as MoS<sub>2</sub>-I<sub>1/3</sub> nanotubes. The MoS<sub>2</sub> -  $x$ -I <sub>$y$</sub> , ( $0 \leq x < 1, y < 1$ ), nanotubes representing the smallest known inorganic nanotubes have been proposed to have a single molecular layer structure. However, their structure differs strongly from known MoS<sub>2</sub> structure and it can not represent a limit structure in the extrapolation toward the minimal diameter and wall thickness.

## 2 Experiments proving the existence of phospholipid nanotubes

It was previously observed [7] that the giant unilamellar phospholipid vesicles prepared by the method proposed by Angelova et al. [40] are rigid and spherical. It was further indicated [7] that the vesicles are connected by thin tubular membranous structures. These indications were drawn from an experiment [7] where a few percent of fluorescent phospholipid NBD-PC was mixed with the unlabelled phospholipid rendering the vesicles fluorescent. A laser beam was applied to the vesicles and suppressed the fluorescence in the affected part of the sample. However, after a

very short time (about 2 minutes) the fluorescence reappeared. Such quick restoration of fluorescence could not happen due to transport of phospholipid through the water solution, therefore it was suggested that the vesicles must be connected by very thin and fragile membraneous structures [7]. These structures were not directly observed, however, tubular connections between vesicles were directly observed in a system subject to osmotic stress [7].

When the vesicles are made of phospholipid POPC and observed under the optical microscope they undergo a slow spontaneous shape transformation in which the difference between the areas of the two layers of the phospholipid membrane diminishes [8]. The mechanism of the shape transformation is not known; the suggested possibilities are the inequality of the chemical potential of the phospholipid molecules in the vesicle membrane and in the solution that causes a slow but continuous loss of the phospholipid molecules from the outer membrane layer into the solution, the drag of the phospholipid molecules from the outer solution of the vesicles by the glass walls of the chamber, by slight evaporation of the liquid caused by imperfect sealing of the chamber by the grease, by chemical modification of the phospholipid molecules and by their flip-flop [8]. Consequently, the tubular structures, if present, would become shorter and thicker with time. We therefore assumed that after a certain period of time the tubular structures (if present) would become thick enough to be visible under the optical microscope. These assumptions proved to be correct. Some time after the solution containing the vesicles is placed into the observation chamber (usually about half an hour) long myelin-like structures appear as attached to the spherical part of the vesicle at one end while the other end is usually free. A small amount of myelin-like vesicles with very low volume to area ratio can also be observed. These myelin-like structures derive from the remnants of the nanotubular network created during the vesicle formation phase in the electroformation chamber; the network is partially torn when the vesicles are rinsed from the chamber.

The description of the experiments proving the existence of phospholipid nanotubes and the results are shown below.

## **2.1 Preparation of phospholipid vesicles connected by nanotubes**

The phospholipid 1-Palmitoyl-2-Oleoyl-sn- Glycero-3-Phosphocholine (POPC) was purchased from Avanti Polar Lipids. The fluorescent phospholipid probe (2-(12-(7-nitrobenz-2-oxa-(1,3-diazol-4-yl)amino) dodecanoyl-1-hexadecanoyl-sn-glycero-3-phosphocholine)) (NBD-PC) was purchased from Molecular Probes, Inc.. Giant phospholipid vesicles were made from POPC and also from the mixture of POPC and 1.5% NBD-PC by the modified method of electroformation[40] as described in[41]. All the described features regarding the shapes of the vesicles were the same in the system with and in the system without the fluorescent probe.

The experiment was performed at room temperature. In the procedure, 20  $\mu$ l of phospholipid (or mixture of phospholipid and fluorescent probe), dissolved in 2:1

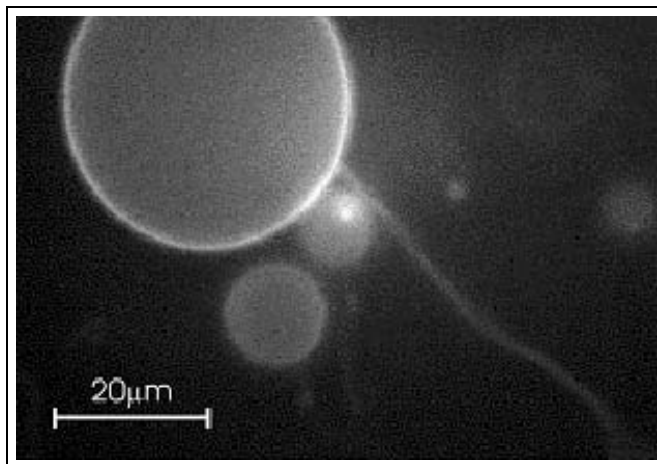


Figure 4: A fluorescence microscope image of the vesicle made of POPC and 1.5% NBD-PC. The length of the myelin-like protrusion was several diameters of the spherical part. The fluorescence measurements were done on the inverted optical microscope (IMT-2, Olympus, Japan), using the reflected light fluorescence attachment IMT2-RFL. The dichroic mirror unit (IMT-DMB) allowed the excitation from 405 to 490 nm and the observation of the fluorescence on the wavelengths higher than 515 nm (from [8]).

chloroform/methanol mixture, was applied to a pair of Pt electrodes. The solvent was allowed to evaporate in low vacuum for two hours. The electrodes were placed 4 mm apart in the electroformation chamber that was filled with 2 ml of 0.2 M sucrose solution (or with 2 ml of pure water). An AC electric field (1 V/mm, frequency 10 Hz) was applied for two hours. Then, the AC field was reduced to (0.75 V/mm, 5 Hz) and applied for 15 min, to (0.5 V/mm, 2 Hz) and applied for 15 min, and to (0.25 V/mm, 1 Hz) and applied for 30 min.

The contents of the chamber were poured out into a plastic beaker. The chamber was then filled with 2 ml 0.2 M glucose solution (or with 2 ml of pure water, respectively) that contained no phospholipid. This solution was also poured out adding to the solution that was already in the plastic beaker. The contents of the plastic beaker were gently mixed by turning the beaker upside down.

Immediately after the preparation, the solution containing the vesicles was placed into the observation chamber made by a pair of cover glasses and sealed by vacuum grease. The vesicles were observed by the phase contrast microscope and by the fluorescence microscope.

## 2.2 Phospholipid vesicles with myelin-like protrusions

Immediately after being placed into the observation chamber the vesicles appeared spherical and had different sizes. The myelin-like protrusions were not visible nor

were the long-wavelength shape fluctuations. The short-wavelength shape fluctuations were barely visible. After a certain period of time (of the order of about half an hour) long thin myelin-like protrusions became visible under the fluorescence microscope (Fig.4) and later also under the phase contrast microscope (Fig.6A). Usually, when recognized, the myelin-like shapes appeared as very thin long tubes connected to the vesicle surface at one end while the movement of the myelin-like shapes indicated that they are otherwise free.

The vesicles were prepared in sugar solution [8] as we wanted to obtain a good focus on the vesicle and on the protrusion: the vesicles were grown in sucrose solution and rinsed out of the electroformation chamber by the glucose solution. The two solutions were equiosmolar, however, as sucrose has larger molecular weight than glucose, the density of the vesicle content was higher than the density of the surrounding solution and the vesicles sunk to the bottom of the observation chamber while the protrusion aligned with it. Thereby a good focus can be obtained simultaneously on the spherical part and on the protrusion.

A possibility was considered that chirality of system constituents might be essential in determination of the stable tubular shape of the protrusion. Namely, a theory was proposed [42] where stable tubular shape was explained on the basis of chirality. It was shown [42] that the stable tubular shape corresponds to the minimum of the membrane free energy obtained by expansion over the curvature and nematic fields. For nonzero chirality parameter, stable tubes were obtained with uniform orientational ordering of bilayer constituents and also with a periodic helical variation in orientational ordering within stripe - like domains. Further, the proposed theory described modulation of the degree of twist of the ribbons formed by dimeric surfactants associated with chiral counterions [6]. It was of our interest to find out whether the chirality of the bilayer constituents is a prerequisite factor that is responsible for the stability of the thin tubular structures of phospholipid membrane. The POPC molecules are not chiral, however, chirality of the constituents may develop also due to their association with the ions or molecules from the adjacent solution [6] (glucose) [9]. In order to clarify this issue the vesicles were prepared and rinsed from the electroformation chamber by pure water. Figure 5A shows a first sight of the vesicle with the protrusion in pure water. The protrusion is barely seen. The mother sphere is floating in the solution while the protrusion is wobbling, so that it is difficult to obtain a focus on the mother sphere and the protrusion at the same time or even to obtain a sharp picture of the protrusion. The line in Fig.5B is drawn to help in locating the protrusion. As stable tubular structures were found also in system containing pure water [9], this experiment supports the notion that chirality is not a prerequisite mechanism for stability of phospholipid nanotubes.

From the above observations (Figs.4,5) we cannot determine the radius of the protrusion. The radius may be much smaller than the width of the shade seen in the pictures. Further, the direction of the slow shape transformation indicates that the protrusion exists before it becomes visible and is therefore then even thinner.

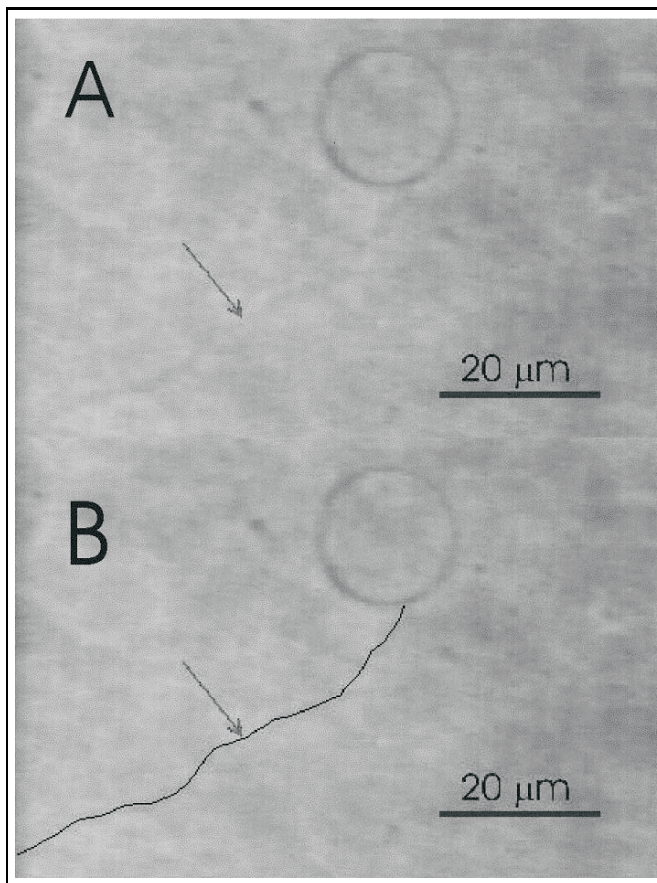


Figure 5: A: A giant phospholipid vesicle (made of POPC in pure water) with long thin tubular protrusion. The vesicle was observed in the closed chamber made of cover glasses, several hours after the preparation. The figure shows the barely visible protrusion, as it is observed in the beginning of the process. B: A duplicate of the picture with a line that is drawn to help in locating the protrusion. The vesicles were observed under the inverted microscope Zeiss IM 35 with the phase contrast optics (from [9]).

The possibility should be considered, that the radius of the tubular protrusion is immediately after the formation very small - of the order of phospholipid bilayer thickness.

### 2.3 Shape transformation of the vesicle with the myelin-like protrusion

A vesicle was chosen and followed for several hours. A typical time course of the shape transformation can be seen in Fig.6. The sequence started from a spherical mother vesicle with a long thin myelin-like protrusion that appeared as a cylinder (A). The barely visible protrusion was perceived about three hours after the solution containing the vesicles was placed into the observation chamber. By the time the myelin-like protrusion thickened and shortened (B,C), while the undulations of the cylinder became noticeable and more pronounced. The mother vesicle remained more or less spherical. In the shortened myelin-like protrusion, the necks seemed to persist while exhibiting oscillations in their width making the final phases of the process to look like the beads were stepwise integrated into the mother vesicle (D,E,F). Finally, the neck of the only remaining daughter vesicle opened (G) yielding a globular vesicle (H). Before opening, the neck widened and shrunk several times. The subsequent transformation of the vesicle into the pear shape and further into the prolate shape was completed in seconds (Fig.6F-H).

The long wavelength fluctuations of the mother vesicle increased with shortening of the myelin-like protrusion and became vigorous when the myelin-like protrusion was completely incorporated into the membrane of the mother vesicle.

## 3 Experiments on inorganic nanotubes

### 3.1 Synthesis of MoS<sub>2</sub> nanotubes

Nanotubes of transition metal dichalcogenides have been firstly synthesized by sulphurisation of transition metal oxides [43]. The longitudinal length of nanotubes was determined by geometry of precursor crystals. The dimensions of precursor crystals dictated the size of nanotubes also during reduction of needle-like transitional metal three-sulphides and recrystallization to disulphide cylindrical structure [44]. They size up to several tens of micrometers in length with diameter from few tens nanometers up to hundreds nanometers. Besides, the dimensions of TMD nanotubes can be controlled using a template method with thermal decomposition of (NH<sub>4</sub>)<sub>2</sub>MoS<sub>4</sub> and (NH<sub>4</sub>)<sub>2</sub>Mo<sub>3</sub>S<sub>13</sub> in porous aluminium oxide membrane [45]. The MoS<sub>2</sub> nanotubes produced by such a way were equal shaped, that were  $\simeq 30$  nm long with diameters of 50 nm and wall thickness of about 10 nm.

Besides by the sized controlled techniques, the MoS<sub>2</sub> nanotubes were synthesised also by chemical transport reaction, which is a standard method for growth

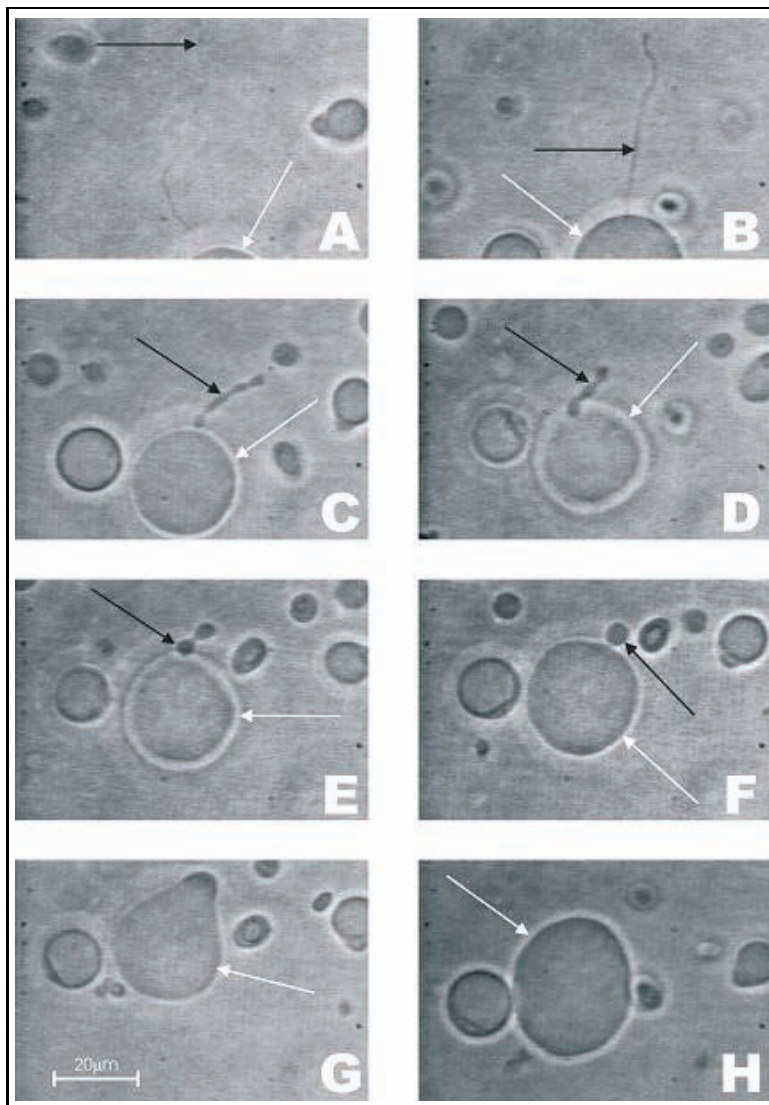


Figure 6: Shape transformation of the giant phospholipid vesicle (made of POPC and 1.5 % NBD-PC) with time. The times after the preparation of the vesicles are A:3 h, B:3h 20 min, C:4 h, D:4 h 2 min, E:4 h 4 min 30 s, F:4 h 8 min 15 s, G:4 h 14 min 25 s, H:4 h 14 min 30 s. The black arrows indicate the protrusion while the white arrows indicate the mother vesicle. The vesicles were observed under the inverted microscope Zeiss IM 35 with the phase contrast optics (from [8]).

of transition metal dichalcogenides [38]. They grow together with strongly undulated plate-like crystals from vapor phase. The nearly equilibrium conditions enable growth with extremely low density of structural defects. The nanotubes of different geometry produced by such a way can be used as a typical example of thermodynamically stable structures.

### 3.2 Chemical transport reaction

The chemical transport reaction is a standard method for growing plate-like crystals of transition metal dichalcogenides in two zone furnace. Modifications of growth parameters, as example temperature, temperature gradient, and/or partial pressures of components in the transport reaction change the crystal growth from plane geometry to cylindrical one. The MoS<sub>2</sub> nanotubes grow at 10<sup>-3</sup> Pa with temperature gradient of 5.6 K/cm [38, 23, 39]. The transport agent, iodine in our case, reacts with transition metal at high temperature (above 1120 K) forming the volatile product, which decomposes at lower temperature (1010 K), where transition metal reacts again with sulphur to solid transition metal disulphide. In three weeks, a few percents of the starting material was transported by the reaction to form nanotubes, while the rest of the transported material grown as strongly undulated thin plate-like crystals.

The origin of undulation of very thin crystal flakes, which constitute the nucleation sites for the tubes, was explained by stacking mismatch between nucleation islands of the rhombohedral and hexagonal stacking causing an appearance of internal strain [39]. When the tube form is nucleated, the tube continues to grow up to relatively large distances, in some cases up to several millimeters. The diameters in multiwall nanotubes range from several micrometers to less than ten nanometers. The growth is rigid resulting in straight tubes of homogeneous diameter.

### 3.3 Collapse

In synthesizing MoS<sub>2</sub> micro and nanotubes, an interesting phenomenon, that we refer to as a collapse, was noted [23]; usually, MoS<sub>2</sub> micro and nanotubes are hollow cylinders composed of many S-Mo-S molecular layers (Fig.7A), however some stable flattened (*i.e.* collapsed) multilayer structures also appear (Fig.7B). Although the MoS<sub>2</sub> tubes are very soft against radial forces, it seems that the collapse is not caused by mechanical manipulation during the sample preparation [23]. The collapse could rather be triggered by an obstacle that would affect the tube growth [23] so that the tube becomes thicker due to increasing number of layers.

## 4 Theoretical description of nanotubes

The systems described above (the phospholipid bilayer and the S – Mo – S molecular layer) can be considered as systems with one of the extensions (thickness) much

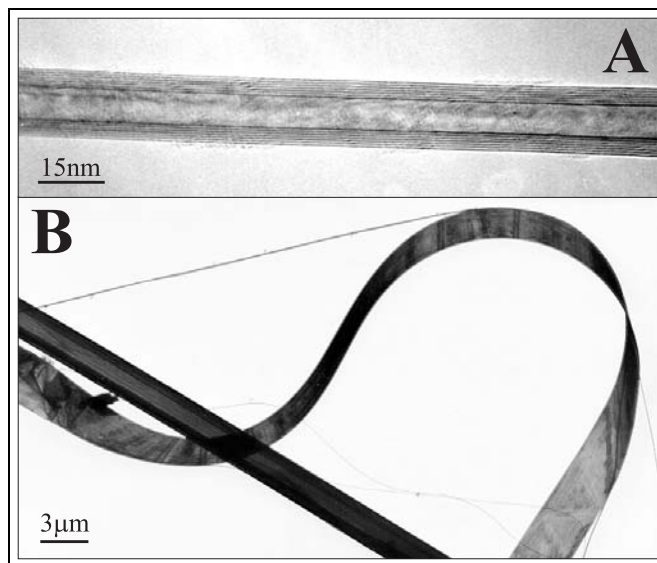


Figure 7: High-resolution transmission electron micrograph of the  $\text{MoS}_2$  nanotube. Dark fringes correspond to molybdenum atomic layers. The nanotube consists of seven  $\text{MoS}_2$  layers (upper); transmission electron micrograph of the collapsed  $\text{MoS}_2$  microtube. The thickness of the tube estimated from the ribbon turn is approximately 70 nm (lower) (from [46]).

smaller than the other two. Therefore the configuration of such system resembles a two-dimensional surface embedded into a three dimensional space.

In describing the shape of the of the system as a shape of a two-dimensional surface in a three dimensional space we should have in mind that our system is really a three-dimensional structure. The system is regarded as composed of particles (building units). These building units act one upon another; the building unit directly perceives the local curvature of the surface. In other words, the energy of the building unit depends on the local curvature of the surface. In our description, such systems can be conveniently described by the curvature of the surface while the “third dimension” is accounted for in the free energy of the system.

It is the main purpose of this contribution to present a simple general theory that can be used for description of nanotubes. This theory is based on the evidence that it is energetically favorable for the material to assemble into tubular shape. It is considered that the intrinsic shape of individual building units (atoms, molecules, small patches) is anisotropic. In deriving the free energy of the system this is taken into account by choosing a relevant reference state. In effect, the classical theory of elasticity of isotropic thin surfaces [47] is upgraded by an additional term referred to as the deviatoric contribution.

In particular, we will use the proposed theory to describe the experiments presented in the previous section.

## 4.1 Curvature field

Let us imagine a surface and chose a point in it. We cut the surface by a plane through the normal to the surface. The intersection forms a curve in space – the normal cut. The curvature of the normal cut at the chosen point is given by the inverse of the radius if the circle that fits the normal cut at the chosen point. There are infinitely many normal cuts that can be made through the chosen point. The curvature of the surface is given by knowing the curvatures of all the normal cuts. The possible normal cuts in general attain the values between the minimal and the maximal value. These extreme curvatures are called the principal curvatures. The respective directions are perpendicular to each other and are called the principal directions. The shape of the surface can be deduced by knowing the curvature of the surface in each point.

In describing the physical structure we must take into account that the “surface” is composed of building units (atoms, molecules, clusters, small patches). The conformation of the building unit is constrained by the interactions of the chosen building unit with its surroundings, e.g. with the neighboring building units. The energy states of the building unit depend on the local curvature of the surface as it is this quantity that determines the mutual configuration of the neighboring building units. We will follow the mean field approach where we assume that the neighboring building units are forming a curvature field and that the energy of a chosen building unit depends on the local curvature field.

If the “surface” were composed of intrinsically equal building units, one could imagine the surface shape that would be energetically the most favorable for the particular kind of building unit. In other words, no energy should be spent to adjust the unit into the surface. We will refer to such shape as a shape intrinsic to the building unit or - intrinsic shape. The intrinsic shape of the building unit depends on the properties of the unit and its interactions with the surroundings. In real systems, we can not necessarily expect that such shape is actually attained, due to various constraints imposed upon the system. For example, when the phospholipid bilayer vesicles are formed in water, the shapes tend to close in order to avoid the contact of the hydrophobic hydrocarbon chains with water. As the surface area and the enclosed volume are fixed, the shape subject to the geometrical constraints cannot have the same curvature in every point. Some (or all) building units must therefore attain energetically less favorable states, i.e. states of higher energy. For some intrinsic shapes, such as the shape of a chosen point of the saddle it is not possible to form a surface that would have equal curvature even in a small region around this point.

We assume that the shapes of nanotubes considered in this contribution are (quasi)equilibrium shapes so that they correspond to the minimum of the relevant thermodynamic potential that depends on the energy state of the system building units. We are seeking the shape of the surface that gives the lowest energy of the whole surface at given constraints imposed upon the system. This problem differs

somewhat from a problem where we are seeking the equilibrium configuration of the system subject to a certain field within a chosen geometry (such as for example a problem of a flat electrical double layer [48, 49, 34]) since in the problem considered in this work the relevant field itself determines the geometry of the system.

## 4.2 The deviatoric elasticity of a surface

We propose that the energy of a single building unit derives from the mismatch between the local shape of the surface and the intrinsic shape of the building unit. The local curvature of the surface is represented by curvatures of all possible normal cuts of the surface through the site of the building unit. In deriving the energy the building unit is treated as dimensionless while the surrounding surface is treated as a continuum. This implies that the building unit behaves as a quadrupole in the curvature field.

The energy of a single building unit energy is given by a phenomenological expression consisting of two terms [50],

$$E = \frac{\xi}{4\pi} \int_0^{2\pi} (C - C_m)^2 d\psi + \frac{\xi^*}{16\pi} \int_0^{2\pi} \left( \frac{d}{d\psi} (C - C_m) \right)^2 d\psi, \quad (1)$$

where  $\xi$  and  $\xi^*$  are positive interaction constants,  $C$  is the curvature of the normal cut that is for an angle  $\psi$  rotated in the principal axes system of the surface,  $C_m$  is the curvature of the normal cut corresponding to the intrinsic shape in the same direction. The first contribution takes into account the differences of the curvatures of the normal cuts of the two systems while the second contribution takes into account the coupling between the neighboring curvatures of the normal cuts of the two systems.

The orientation of the building unit is described by considering that the principal directions of the surface are in general different from the principal directions of the intrinsic shape. The mutual orientation of the two systems is determined by the angle  $\omega$ . We consider the Euler equations for the curvatures of the respective normal cuts of the continuum

$$C = C_1 \cos^2 \psi + C_2 \sin^2 \psi \quad (2)$$

and

$$C_m = C_{1m} \cos^2(\psi + \omega) + C_{2m} \sin^2(\psi + \omega), \quad (3)$$

where  $C_1$  and  $C_2$  are the principal curvatures describing the local shape of the surface, and  $C_{1m}$  and  $C_{2m}$  are the principal curvatures describing the intrinsic shape.

By performing the necessary integrations in Eq.(1) we get

$$E(\omega) = \frac{\xi}{2} (H - H_m)^2 + \frac{1}{2} \frac{\xi + \xi^*}{2} (\hat{C}^2 - 2\hat{C}\hat{C}_m \cos(2\omega) + \hat{C}_m^2), \quad (4)$$

where

$$H = \frac{1}{2} (C_1 + C_2), \quad (5)$$

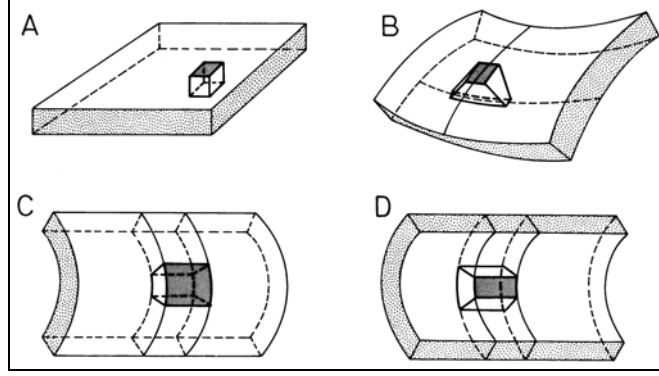


Figure 8: A schematic presentation of four different intrinsic shapes: A: flat shape ( $H_m = \hat{C}_m = 0$ ), B: saddle shape ( $H_m \neq 0, \hat{C}_m \neq 0$ ), C: cylinder ( $H_m > 0, |\hat{C}_m| = H_m$ ), D: inverted cylinder ( $H_m < 0, |\hat{C}_m| = -H_m$ ). The shape A is isotropic while the shapes B, C and D are anisotropic (from [9]).

$$\hat{C} = \frac{1}{2}(C_1 - C_2), \quad (6)$$

$$H_m = \frac{1}{2}(C_{1m} + C_{2m}) \quad (7)$$

and

$$\hat{C}_m = \frac{1}{2}(C_{1m} - C_{2m}). \quad (8)$$

The quantities  $H$  and  $H_m$  are the mean curvatures of the local membrane shape and of the intrinsic shape, respectively, while the quantities  $\hat{C}$  and  $\hat{C}_m$  represent the difference between the two principal curvatures of the local membrane shape and of the intrinsic shape, respectively.

The building unit is called isotropic if  $C_{1m} = C_{2m}$  while it is called anisotropic if  $C_{1m} \neq C_{2m}$ . Fig. 8 gives a schematic presentation of four different intrinsic shapes.

The expression (4) can be derived also in an elegant way by curvature tensors  $\underline{C}$  and  $\underline{C}_m$ . At the site of the chosen building unit the surface shape is described by the diagonalized curvature tensor  $\underline{C}$ ,

$$\underline{C} = \begin{bmatrix} C_1 & 0 \\ 0 & C_2 \end{bmatrix}, \quad (9)$$

while the intrinsic shape is described by the diagonalized curvature tensor  $\underline{C}_m$

$$\underline{C}_m = \begin{bmatrix} C_{1m} & 0 \\ 0 & C_{2m} \end{bmatrix}. \quad (10)$$

The principal directions of the tensor  $\underline{C}$  are in general different from the principal directions of the tensor  $\underline{C}_m$ , the systems being mutually rotated by an angle  $\omega$ .

We introduce the mismatch tensor  $\underline{M}$  [46],

$$\underline{M} = \underline{R} \underline{C}_m \underline{R}^{-1} - \underline{C} \quad (11)$$

where  $\underline{R}$  is the rotation matrix,

$$\underline{R} = \begin{bmatrix} \cos \omega & -\sin \omega \\ \sin \omega & \cos \omega \end{bmatrix}. \quad (12)$$

The single-building unit is determined by terms composed of two invariants of the mismatch tensor  $\underline{M}$ . Terms up to the second order in the tensor elements are taken into account. The trace and the determinant are considered as the fundamental invariants [46],

$$E = \frac{K}{2} (\text{Tr}(\underline{M}))^2 + \bar{K} \text{Det}(\underline{M}), \quad (13)$$

where  $K$  and  $\bar{K}$  are constants. Performing the necessary operations and using the expressions (9) - (13) yields the expression for the single-building unit energy (Eq. 4)

$$E = \frac{\xi}{2} (H - H_m)^2 + \frac{\xi + \xi^*}{4} (\hat{C}^2 - 2\hat{C}_m \hat{C} \cos(2\omega) + \hat{C}_m^2). \quad (14)$$

The constants used in Eq.(14) are

$$\xi = 2\bar{K} + 4K \quad (15)$$

and

$$\xi^* = -6\bar{K} - 4K. \quad (16)$$

It can be seen in Eq.(14) that the energy  $E$  depends on the angle  $\omega$  coupled to the difference between the two intrinsic curvatures  $\hat{C}_m$ . This means that for anisotropic building units, the orientation with respect to the surface coordinate system is important.

#### 4.2.1 Building units that are free to rotate within the surface plane

If the units are free to rotate within the surface, all orientations do not have the same energy and it can be expected that the building unit would spend on the average more time in the orientation that is energetically more favorable. If it is assumed that the building unit can attain any orientation from 0 to  $2\pi$ , the partition function of a single building unit ( $q$ ) is [51]

$$q = \frac{1}{\omega_0} \int_0^{2\pi} \exp\left(-\frac{E(\omega)}{kT}\right) d\omega, \quad (17)$$

with  $\omega_0$  an arbitrary angle quantum and  $k$  the Boltzmann constant. In the partition function of the building unit the contribution of the orientational states  $q_{\text{orient}}$  is distinguished from the contribution of the other states  $q_c$ ,  $q = q_c q_{\text{orient}}$  [50],

$$q_c = \exp\left(-\frac{\xi}{2kT}(H - H_m)^2 - \frac{\xi + \xi^*}{4kT}(\hat{C}^2 + \hat{C}_m^2)\right), \quad (18)$$

$$q_{\text{orient}} = \frac{1}{\omega_0} \int_0^{2\pi} \exp\left(\frac{(\xi + \xi^*)\hat{C}_m \hat{C} \cos(2\omega)}{2kT}\right) d\omega. \quad (19)$$

Integration in Eq. (19) over  $\omega$  yields

$$q_{\text{orient}} = \frac{1}{\omega_0} I_0\left(\frac{(\xi + \xi^*)\hat{C}_m \hat{C}}{2kT}\right), \quad (20)$$

where  $I_0$  is the modified Bessel function. The free energy of the building unit is then obtained by the expression

$$F_u = -kT \ln q, \quad (21)$$

which yields [50] ,

$$F_u = \frac{\xi}{2}(H - H_m)^2 + \frac{\xi + \xi^*}{4}(\hat{C}^2 + \hat{C}_m^2) - kT \ln\left(I_0\left(\frac{(\xi + \xi^*)\hat{C}_m \hat{C}}{2kT}\right)\right). \quad (22)$$

Since the modified Bessel function and the quadratic function are even functions of the difference  $\hat{C}$ , the difference  $\hat{C}$  can be in (Eq.(22)) replaced by the curvature deviator  $D$

$$D = |\hat{C}| \quad (23)$$

that is an invariant of the curvature tensor as it can be expressed by its trace and determinant,

$$D = \sqrt{(\text{Tr}(\underline{C})/2)^2 - \text{Det}(\underline{C})}. \quad (24)$$

Considering that

$$\text{Tr}(\underline{C}) = 2H \quad (25)$$

and

$$\text{Det}(\underline{C}) = C_1 C_2. \quad (26)$$

it follows that

$$D = \sqrt{H^2 - C_1 C_2}. \quad (27)$$

Thereby the free energy of a single building unit is expressed in a simple and transparent way by two independent invariants of the curvature tensor: the trace and the absolute value of the difference of the main curvatures *i.e.* by the mean curvature  $H$  and the curvature deviator  $D$ ,

$$F_u = \frac{\xi}{2}(H - H_m)^2 + \frac{\xi + \xi^*}{4}(D^2 + D_m^2) - kT \ln\left(I_0\left(\frac{(\xi + \xi^*)D_m D}{2kT}\right)\right), \quad (28)$$

where

$$D_m = \sqrt{H_m^2 - C_{1m}C_{2m}}. \quad (29)$$

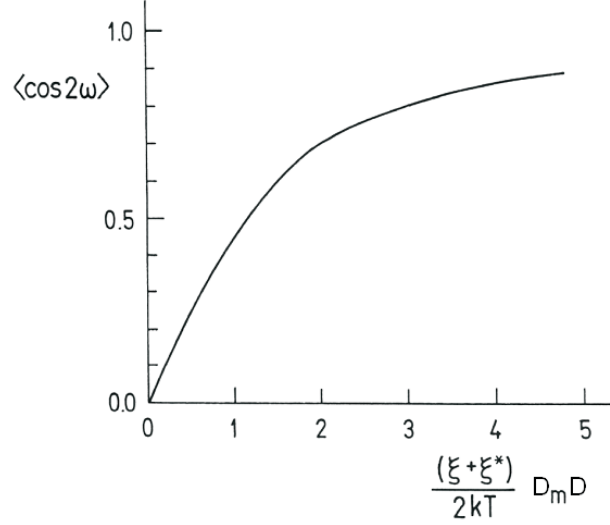


Figure 9: Average orientation of the building unit  $\langle \cos(2\omega) \rangle$  as a function of the curvature deviator  $D$  (from [52]).

The average orientation of the building unit may be given by  $\langle \cos(2\omega) \rangle$  [52],

$$\langle \cos(2\omega) \rangle = \frac{I_1 \left( \frac{(\xi + \xi^*) D_m D}{2kT} \right)}{I_0 \left( \frac{(\xi + \xi^*) D_m D}{2kT} \right)}. \quad (30)$$

where  $I_1$  is the modified Bessel function.

Fig. 9 shows the average orientation of the anisotropic building unit as a function of the curvature deviator  $D$ . For small  $D$ , *i.e.* in nearly isotropic regions, the units are randomly oriented. The orientational ordering increases with increasing  $D$  and approaches the state where all the units are aligned at large  $D$ , *i.e.* in strongly anisotropic regions.

### 4.3 Determination of stability of phospholipid nanotubes by deviatoric elasticity

It is assumed that the stable shape of the phospholipid vesicle is determined by the minimum of the free energy of the phospholipid bilayer. A variational problem is stated where we require that the variation of the free energy with respect to the curvature field vanishes at given constraints. The principal curvatures as functions of the position are the relevant extremales. A rigorous solution of the variational problem would be obtained by stating and solving the corresponding Euler-Lagrange equations [53]. However, at the present state of knowledge it is more appropriate to

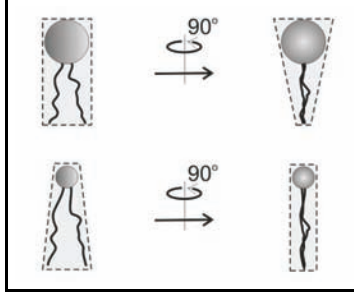


Figure 10: Schematic representation of the intrinsic anisotropy of phospholipid molecules in the phospholipid layer. Two kinds of phospholipid molecules are presented where the anisotropy derives from the tail structure. Front and side view are shown.

estimate the behavior of the system by applying an adjustable parametrical ansatz for the shape. As in this contribution we are focusing on the general properties of the system and not on the details of the shape we will not consider the rigorous solution of the variational problem but will rather follow the method based on the parametrical model.

First we must write the relevant free energy and geometrical constraints. It is taken that a single phospholipid molecule represents the building unit of the surface. It is accounted for that in the phospholipid bilayer there are two opposing surfaces that are in close contact. It is considered that the phospholipid molecules are due to their structure anisotropic with respect to the axis pointing in the direction of the normal to the bilayer (Fig.10). They are free to rotate within the plane of the bilayer [34], however, at given site of the molecule (given local curvature of the layer) it could be expected that different orientational states have different energies and that the molecule would spend on the average more time in the configuration with lower energy. It is therefore appropriate to use Eq.(28) to calculate the contribution of a single phospholipid molecule to the free energy of the bilayer.

In the first approximation the free energy of the phospholipid bilayer is obtained by summing the contributions of the individual phospholipid molecules of both layers,

$$F = \int n_{\text{out}} F_u(C_1, C_2) dA + \int n_{\text{in}} F_u(-C_1, -C_2) dA, \quad (31)$$

where  $n_{\text{out}}$  and  $n_{\text{in}}$  are the area densities of the molecules in the outer and the inner layer, respectively. The integration is performed over the bilayer area  $A$ . Note that the principal curvatures in the inner layer have the sign opposite to the sign of the principal curvatures of the outer layer due to the specific configuration of the phospholipid molecules within the layers - touching by the tails.

If we assume for simplicity that the area densities are constant over the respective layers and also equal  $n_{\text{out}} = n_{\text{in}} = n_0$ , and insert the expression for the single-unit

energy (Eq.(28)) into Eq.(31), we obtain [9]

$$F = n_0\xi \int H^2 dA + n_0 \frac{\xi + \xi^*}{2} \int D^2 dA - 2n_0 kT \int \ln \left( I_0 \left( \frac{\xi + \xi^*}{2kT} DD_m \right) \right) dA. \quad (32)$$

In integrating, the differences in the areas of the inner and the outer layer were disregarded, so that the contributions proportional to the intrinsic mean curvature  $H_m$  of the inner and the outer layer cancelled and there is no spontaneous curvature for the bilayer vesicles composed of a single species of molecules. Also, in Eq.(32), the constant terms were omitted.

It follows from Eq.(32) that the free energy of the phospholipid bilayer is expressed by two first-order invariants of the curvature tensor - trace ( $2H$ ) and deviator ( $D$ ).

#### 4.3.1 Thermodynamic link

The first and the second term of Eq.(32) can be combined by using the connection between  $H$  and  $D$  following from Eq.(27),

$$H^2 = D^2 + C_1 C_2, \quad (33)$$

to yield [9]

$$F = W_b + F_d, \quad (34)$$

where

$$W_b = n_0 \frac{3\xi + \xi^*}{8} \int (2H)^2 dA - n_0 \frac{\xi + \xi^*}{2} \int C_1 C_2 dA \quad (35)$$

and

$$F_d = -2kT n_0 \int \ln \left( I_0 \left( \frac{\xi + \xi^*}{2kT} DD_m \right) \right) dA. \quad (36)$$

The obtained expressions (34) - (36) are compared to the local bending energy of a thin, almost flat, laterally isotropic continuum (local bending energy of isotropic continuum) [47, 54]

$$W_b = \frac{k_c}{2} \int (2H)^2 dA + k_G \int C_1 C_2 dA, \quad (37)$$

where  $k_c$  and  $k_G$  are the membrane local and Gaussian bending constants, respectively. We can see that the statistical mechanical derivation (Eq.(32)) recovers the expression (37), where

$$n_0(3\xi + \xi^*)/4 = k_c \quad (38)$$

and

$$-n_0(\xi + \xi^*)/2 = k_G, \quad (39)$$

and yields also an additional contribution (Eq.(36)) due to the orientational ordering of the phospholipid molecules. This contribution which is always negative is called the deviatoric elastic energy of the membrane (originating in the curvature deviator  $D$ ). It can also be seen that the constant before the Gaussian curvature in Eq.(35) is negative.

For isotropic building units  $D_m = 0$ . Taking into account that  $I_0(0) = 1$  it follows from Eq.(36) that

$$F_d(D_m = 0) = 0 \quad (40)$$

and from Eq.(34)

$$F(D_m = 0) = W_b. \quad (41)$$

It follows from Eqs.(40), (41), (32) and (37) that for isotropic building units the free energy of the system can be expressed in an equally transparent way by either set of invariants of the curvature tensor: trace and determinant or trace and deviator (see also Eqs.(25)-(27)).

Introducing the dimensionless quantities, the energy  $F$  (Eq.(34)) and its terms (Eqs.(35) and (36)) are normalized by  $2\pi n_0(3\xi + \xi^*)$ ,

$$f = w_b + f_d, \quad (42)$$

$$w_b = \frac{1}{4} \int (2h)^2 da + \kappa_G \int c_1 c_2 da, \quad (43)$$

$$f_d = -\kappa \int \ln(I_0(\vartheta d_m d)) da, \quad (44)$$

where

$$da = dA/4\pi R^2, \quad (45)$$

$$R = (A/4\pi)^{1/2}, \quad (46)$$

$$\kappa_G = -(\xi + \xi^*)/(3\xi + \xi^*), \quad (47)$$

$$\kappa = 4kTR^2/(3\xi + \xi^*), \quad (48)$$

$$\vartheta = (\xi + \xi^*)/2kTR^2, \quad (49)$$

$$c_1 = RC_1, \quad (50)$$

$$c_2 = RC_2, \quad (51)$$

$$h = RH, \quad (52)$$

$$d = RD \quad (53)$$

and

$$d_m = RD_m. \quad (54)$$

Alternatively, we obtain the dimensionless local bending energy of isotropic continuum (Eq.(43)) if we normalize the expression (37) by  $8\pi k_c$ . Thereby,

$$\kappa_G = k_G/2k_c. \quad (55)$$

To estimate the interaction constants, we assume that the conformation of the phospholipid molecules is equal all over the membrane and take for simplicity that  $\xi = \xi^*$ . In this case,  $\kappa_G = -1/2$ . It follows then from Eq.(55) that  $k_G = -k_c$ . By comparing the constants before the first terms of Eqs.(35) and (37) we can express the interaction constant  $\xi$  by the measured quantities: the local bending constant  $k_c$  and the area density of the number of phospholipid molecules  $n_0$ , so that

$$\xi = k_c/n_0. \quad (56)$$

It follows from Eqs.(48) or (49) and (56) that

$$\kappa = 1/\vartheta = kTR^2n_0/k_c. \quad (57)$$

We consider that  $k_c \simeq 20kT$  [55, 56] and that  $n_0 = 1/a_0$  where  $a_0$  is the area per molecule,  $a_0 \simeq 0.6\text{nm}^2$  [34],  $T = 300\text{K}$  and  $R = 10^{-5}\text{m}$ . This gives  $\kappa = 1/\vartheta \simeq 8.3 \cdot 10^6$ . We estimate that the upper bound of  $D_m$  is the inverse of the molecular dimension ( $\simeq 10^8 \text{ m}^{-1}$ ) so that in our case  $d_m = RD_m$  would be of the order  $10^3$ .

### 4.3.2 Determination of the equilibrium shape of the phospholipid vesicle with thin protrusion

The equilibrium shape is determined by the minimum of the membrane free energy (Eqs.(34)-(36)). The relevant geometrical constraints are taken into account: the bilayer area  $A$  and the enclosed volume  $V$  are fixed,

$$A = \int dA, \quad (58)$$

$$V = \int dV. \quad (59)$$

Considering the bilayer couple principle [57, 58, 59] another constraint requires that the difference between the two membrane layer areas  $\Delta A$  is fixed [60],

$$\Delta A = \delta \int (2H)dA, \quad (60)$$

where  $\delta$  is the distance between the two layer neutral areas. In expression (60) it is taken that  $\delta$  is small with respect to  $1/H$ . The quantity  $\Delta A$  is assumed to reflect the conditions in which the vesicle formation took place and is determined for example by the number of the phospholipid molecules that constitute the respective layers.

The membrane area, the enclosed volume and the area difference (Eq.(60)) are also given in dimensionless form. According to the choice of unit length  $R$  (Eq.(46)), the dimensionless membrane area is

$$a = 1, \quad (61)$$

the dimensionless volume (*i.e.* the relative volume) is

$$v = (36\pi V^2/A^3)^{1/2} \quad (62)$$

while the area difference  $\Delta A$  is normalized by  $8\pi\delta R$  to yield the dimensionless form

$$\Delta a = \int h da. \quad (63)$$

To determine the equilibrium shape, we will due to simplicity compare two shapes that represent the limits of the class of shapes with the long thin protrusion. In the first case the protrusion consists of equal small spheres (Fig.11A) while in the second case the protrusion consists of a cylinder closed by hemispherical caps (Fig.11B). It is expected that these two limit shapes are continuously connected by a sequence of shapes with decreasingly exhibited undulations of the protrusion. As we focus on the general behavior of the system we do not consider the intermediate shapes explicitly.

Each of these two limit cases involves three geometrical model parameters (Fig.11). In the shape with small spheres these parameters are the radius of spherical mother vesicle  $R_{\text{sph}}$ , the radius of small spheres  $r_{\text{sph}}$  and the number of small spheres  $N$  (Fig.11A). As in long thin protrusions  $N$  is expected to be large, any real number is allowed for the parameter  $N$ . In the shape with the cylinder these parameters are the radius of spherical mother vesicle  $R_{\text{scyl}}$ , the radius of the cylinder and the closing hemispheres  $r_{\text{cyl}}$ , and the length of the cylinder  $l$  (Fig.11B).

From geometrical constraints for the relative area (Eq.61), the relative volume  $v$  (Eq.(62)) and the relative area difference  $\Delta a$  (Eq.(63)) the three parameters that determine the shape in both cases (the radius of the mother sphere ( $R_{\text{sph}}/R_{\text{cyl}}$ ), the radius of small spheres/cylinder ( $r_{\text{sph}}/r_{\text{cyl}}$ ) and the number of small spheres/length of the cylinder ( $N/l$ ) are derived.

It is taken that the relative volume is close to 1. For the shape with small spheres, the radius of the mother sphere  $R_{\text{sph}}$  is

$$R_{\text{sph}} \simeq 1 - x, \quad (64)$$

where  $x$  is small. Fulfilling the constraints by keeping the terms of the lowest order in  $x$  yields

$$R_{\text{sph}} = \frac{2+v}{3}, \quad (65)$$

$$r_{\text{sph}} = \frac{2(1-v)}{3(\Delta a - \frac{2+v}{3})}, \quad (66)$$

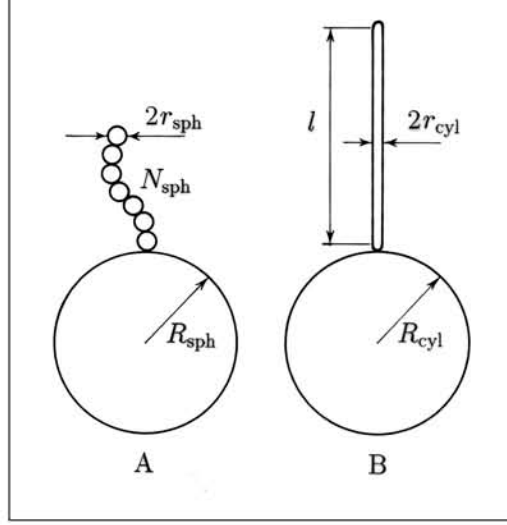


Figure 11: Schematic presentation of the shape composed of the mother sphere and the protrusion composed of small spheres connected by infinitesimal necks (A) and of the shape composed of the mother sphere and thin cylinder closed by hemispherical caps (B).

$$N = \frac{3(\Delta a - \frac{2+v}{3})^2}{2(1-v)}, \quad (67)$$

Analogously, it is taken for the shape with the cylinder that

$$R_{\text{cyl}} \simeq 1 - x \quad (68)$$

which yields

$$R_{\text{cyl}} = \frac{2+v}{3}, \quad (69)$$

$$r_{\text{cyl}} = \frac{(1-v)}{3(\Delta a - \frac{2+v}{3})}, \quad (70)$$

$$l = 4(\Delta a - \frac{2+v}{3}). \quad (71)$$

Within the above approximation ( $v \simeq 1$ ) the relative radius of the mother vesicle is equal to  $(2+v)/3$  in both cases (Eqs.(65) and (69)).

The relative free energy of the membrane is calculated by applying Eqs.(42)-(44) to the respective geometries.

If the deviatoric term were not taken into account the shape with the beadlike protrusion would yield

$$w_{\text{b,sph}} = 1 + N + \kappa_G, \quad (72)$$

while the shape with the cylindrical protrusion would yield

$$w_{b,cyl} = 2 + \frac{l}{8r_{cyl}} + \kappa_G. \quad (73)$$

As the topology of both shapes is the same, the respective Gaussian terms are equal. By inserting  $N$  from Eq.(67),  $l$  from Eq.(71) and  $r_{cyl}$  from Eq.(70), we can see that

$$w_{b,cyl} = w_{b,sph} + 1. \quad (74)$$

It follows from Eq.(74) that within the elasticity theory of the isotropic bilayer membrane, the shape with the protrusion composed of small spheres that are connected with infinitesimal necks would always be favored over the shape with the tubular protrusion. Therefore, this theory is unable to explain stable tubular protrusions.

In considering the deviatoric effect, we assume that there is no deviatoric contribution in the shape composed of spheres connected by infinitesimal necks. At spherical parts there is no deviatoric contribution as the local deviator is equal to zero. In the infinitesimal neck, the curvature deviator is very large, however, the area of the neck is very small. Numerical calculations of the membrane free energy of the shape sequence leading to two spheres connected by infinitesimal neck have shown that as the limit shape is approached, the deviatoric contribution of the neck diminishes [50]. Therefore, for the shape composed of spheres connected by infinitesimal necks the free energy is expressed by Eq.(72).

In the shape with the cylindrical protrusion we consider the deviatoric contribution of the cylindrical part. There is no deviatoric contribution of the neck connecting the mother sphere and the protrusion, on the spherical caps of the protrusion and on the mother sphere. As the relative deviator  $d = 1/2r_{cyl}$  is constant over the area of the cylindrical part  $r_{cyl}l/2$ , we obtain by using Eqs.(44) and (70) [9]

$$f_{d,cyl} = -\frac{2}{3}\kappa(1-v) \ln \left( I_0 \left( \frac{\vartheta d_m 3(\Delta a - \frac{2+v}{3})}{2(1-v)} \right) \right). \quad (75)$$

By choosing the parameters  $v$  and  $\Delta a$ , the geometrical parameters for both shapes (Fig.11, A and B) are determined (Eqs.(65)-(67) and (69)-(71), respectively), and the energies for both shapes are calculated. The values of the free energies are then compared in order to determine which shape yields the lowest membrane free energy at chosen  $v$  and  $\Delta a$ . If  $\Delta a$  is chosen to be high the shape has a long protrusion. As the membrane area and the enclosed volume are fixed, this protrusion is very thin and consequently its mean curvature is large. For the tubular protrusions the deviatoric contribution is large enough to compensate for the less favorable isotropic local bending energy of the cylinder. On the other hand, for lower  $\Delta a$ , the protrusion of the same membrane area and enclosed volume is shorter and broader, therefore its mean curvature is lower. The corresponding deviatoric term of the cylinder is too small to be of importance and the shape with the beadlike protrusion has lower

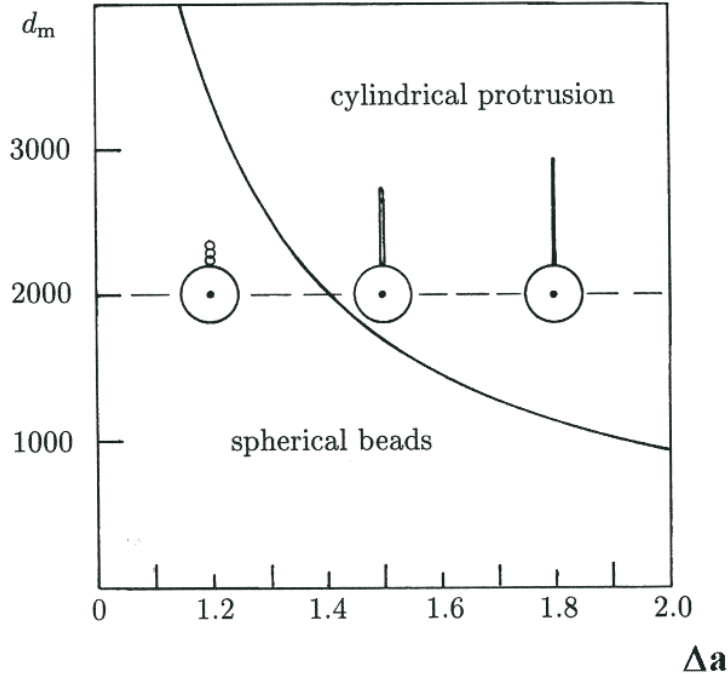


Figure 12: A  $(d_m, \Delta a)$  phase diagram of calculated equilibrium shapes with protrusions. The regions where the shapes with the respective kind of protrusions are energetically more favorable are marked. The sequence of shapes shown in the figure indicates the process of diminishing  $\Delta a$  at constant  $v$  that could be observed in experiment (Fig.6). It was considered that  $a_0 = 0.6 \text{ nm}^2$ ,  $R = 10^{-5} \text{ m}$ ,  $k_c = 20 \text{ kT}$ , so that  $\kappa = 1/\vartheta = 8.3 \cdot 10^6$  while  $v = 0.95$  (see text). The shapes corresponding to different  $\Delta a$  are depicted with the center of the spherical part at the respective  $\Delta a$  values (from [9]).

free energy. At a chosen intrinsic anisotropy  $d_m$ , the shapes with small spheres are energetically more favorable below a certain  $\Delta a$  while above this threshold the shapes with cylinders are favored.

Fig.12 shows the  $(d_m, \Delta a)$  phase diagram exhibiting the regions corresponding to the calculated stable shapes composed of the spherical mother vesicle and tubular protrusion and to the stable shapes composed of the spherical mother vesicle and the protrusion consisting of small spheres connected by infinitesimal necks.

The calculated geometrical parameters and energy contributions for the three shapes depicted in Fig.12 are given in Table 1. The deviatoric contribution of the shape with the cylinder is given also in  $kT$  units. It can be seen that the corresponding deviatoric energies are larger than the estimated energy of thermal

$\Delta a$	$r_{\text{sph}}$	$N$	$f_{\text{sph}}$	$r_{\text{cyl}}$	$l$	$f_{\text{cyl}}$	$f_{\text{dev}}$	$F_{\text{dev}}/kT$
1.3	0.100	3.0	4.0	0.050	1.27	4.65	-0.36	-181
1.6	0.054	11.41	12.41	0.027	2.47	12.04	-1.37	-688
1.9	0.036	25.21	26.21	0.018	3.67	24.18	-3.02	-1520

Table 1: The geometrical parameters and the energies of the shapes depicted in Fig.2:  $\Delta a$ : the normalized difference between the two membrane layer areas,  $r_{\text{sph}}$ : the normalized radius of the small spheres,  $N$ : the number of small spheres,  $f_{\text{sph}}$ : the normalized free energy of the shape with spherical beads,  $l$ : the normalized length of the cylindrical part of the protrusion,  $f_{\text{cyl}}$ : the normalized free energy of the shape with the cylindrical protrusion,  $f_{\text{dev}}$ : the normalized deviatoric contribution to the membrane free energy of the cylindrical protrusion,  $F_{\text{dev}}/kT$ : the deviatoric contribution to the membrane free energy in  $kT$  units. The data used in calculation are  $k_c = 20kT$ ,  $a_0 = 0.6\text{nm}^2$ ,  $R = 10^{-5}$  m,  $v = 0.95$ ,  $d_m = 1000$ , which gives  $\kappa = 1/\vartheta = 8.3 \cdot 10^6$  and  $R_{\text{sph}} = R_{\text{cyl}} = 0.98$  (from [9]).

fluctuations. It can also be seen from Table 1 that for this particular choice of the parameters the dimensionless radius of the stable cylindrical protrusions is about 0.02 - 0.04 which means that the corresponding cylinder radius would be about 200 - 400 nm.

The sequence of shapes shown in Fig.12 roughly simulates the transformation observed in the experiment (Fig.6). Initially,  $\Delta a$  is large and the shape is composed of a mother sphere and long thin nanotube. Assuming that the volume of the vesicle remains constant, the number of phospholipid molecules in the outer layer diminishes with time, therefore  $\Delta a$  decreases and the tubular protrusion becomes thicker and shorter. In the experiment [8], the undulations of the protrusion become increasingly noticeable along the process. Our theoretical results shown in Fig.12 exhibit a discontinuous transition from the tubular protrusion to the protrusion composed of small spheres connected by infinitesimal necks as we consider only the limits of the given class of shapes. Therefore, the phase diagram and the sequence (Fig.12) should be viewed only as an indication to the tendency of the shape transition and not to the details of the shape.

#### 4.3.3 Discussion on the stability of phospholipid nanotubes attached to the mother globule

It follows from the above analysis that the deviatoric contribution to the membrane free energy is considerable only in those regions of the vesicle shape where there is a large absolute value of the difference between the two principal curvatures ( $1/D$  of the order of micrometer or smaller). Elsewhere the deviatoric contribution is negligible. Further, for  $1/D$  down to tenths of nanometers, the argument of the Bessel function can be approximated by an expansion  $I_0(x) \simeq 1 + x^2/4$ . Also,

the logarithmic function in Eq.(44) can be expanded up to linear term to yield the dimensionless local bending energy of isotropic continuum with renormalized constants

$$f = \frac{1}{4}(1 - \frac{1}{4}\vartheta d_m^2) \int (2h)^2 da + (\kappa_G + \frac{1}{4}\vartheta d_m^2) \int c_1 c_2 da. \quad (76)$$

It was taken into account that (Eq.(27))

$$d^2 = h^2 - c_1 c_2. \quad (77)$$

We have used in our calculations presented in Fig.12 and in Table 1 the modified Bessel function, however, we have checked the results also by using Eq.(76) for the shape with the cylindrical protrusion. There was no difference between the results obtained both ways. Therefore for the considered tubular shapes the isotropic local bending energy (Eqs.(37) and (43)) with renormalized constants can be used. It should however be outlined that in the shape with the protrusion composed of small spheres connected by infinitesimal necks such renormalization cannot be used as in the infinitesimal necks the local deviator increases beyond limit. As stated above, the numerical results indicate that there is no contribution of the infinitesimal necks to the free energy. There is also no deviatoric contribution from the spherical parts as the local deviator is there equal to 0. Therefore in the case of spherical beads the isotropic local bending energy (Eq.(43)) with original constants is used,

$$f = \frac{1}{4} \int (2h)^2 da + \kappa_G \int c_1 c_2 da. \quad (78)$$

Although the form of the energy is the same in both cases, there is a difference in the energy due to renormalization of the constants in the case of the shape with cylindrical protrusion (see Eq.(76)). Also, it can be seen that the Gaussian term should be considered too as the Gaussian bending constant is renormalized in the case of nonzero deviatoric contribution. For example, if Eq.(76) is used for a single sphere where  $c_1 = c_2 = 1/r$  and  $r$  is the normalized radius of the sphere, the terms due to renormalization cancel leaving the free energy in the form of Eq.(78). In other words, if the deviatoric effect is taken into account by renormalized isotropic local bending energy (Eq. (43)), the respective shapes that have the same topology, may have different Gaussian contributions.

The mechanism of the spontaneous shape transformation that was observed in experiments [8] remains largely obscure. The tubular character of the protrusions may persist even when the protrusions become thicker while more peculiar shapes with undulated protrusions can also be found (Fig.13). Also, the timing of the transformation may vary from minutes to hours, as the protrusions are initially of very different lengths (Fig.13). If the tubular protrusion becomes thicker in the process of the spontaneous shape transformation the curvature decreases and the deviatoric contribution may become negligible, unless the protrusion develops necks that render minima in the  $f(\Delta a)$  curve [50]. Indeed, oscillations of the neck width

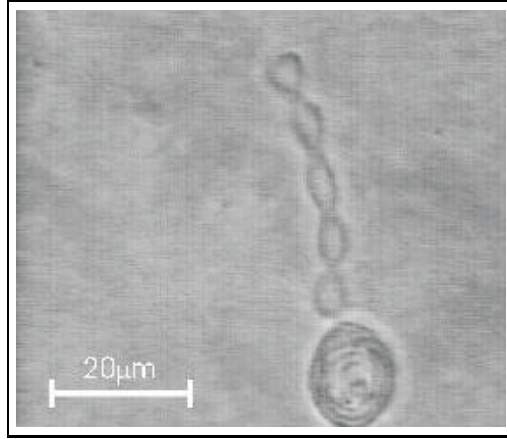


Figure 13: A giant phospholipid vesicle (made of POPC in pure water). Note undulations of the protrusion and a multi-lamellar structure inside the globular part. The vesicle was observed several hours after the solution containing the vesicles was placed into the observation chamber under the inverted microscope Zeiss IM 35 with the phase contrast optics (from [9]).

with time were observed, indicating increased stability of the necks (not shown). A similar effect - the persistence of the neck connecting a spherical daughter vesicle and a mother vesicle was observed also in the opening of the neck induced by cooling while the formation of the neck by heating was quick and took place at higher temperature, indicating the hysteresis [61]. The undulations of the protrusion producing narrow but finite necks could therefore provide a mechanism that would also in the shapes of lower  $\Delta a$  keep the curvature deviator as high as possible and therefore the membrane free energy as low as possible.

It was suggested already by Fischer [62, 63] that the phospholipid molecules with two hydrocarbon chains are in general anisotropic despite of the motion of their segments within the membrane layer. Based on decomposition of the elastic continuum into isotropic and deviatoric bending, he proposed an expression for the membrane local free energy

$$F = 2B_s \int (H - C_0/2)^2 dA + 2B_a \int (|D| - \theta)^2 dA, \quad (79)$$

where  $B_s$  and  $B_a$  are the constants of local isotropic and deviatoric bending, respectively,  $C_0$  is the spontaneous curvature of the membrane and  $\theta$  is the spontaneous warp. The spontaneous warp should originate from the anisotropy of the constituent molecules. However, he then claimed that spontaneous warp is negligible for one component phospholipid membrane due to the fact that the membrane of such vesicle, as observed in experiments, is locally flat. He argued that for a nonzero spontaneous warp the membrane would be corrugated. Experimental results presenting

shapes with tubular protrusions [8, 9] show that the membrane is not flat. However, the bilayer is organized rather in few longer protrusions than in numerous shorter folds. This seems to be energetically more favorable taking into account that the beginning and the end of the protrusion have high local bending energy of isotropic continuum. It must be also considered that the shape of the vesicle is subject to constraints regarding the membrane area, enclosed volume and the numbers of the molecules constituting both layers. The shape with folds would have considerably lower relative volume and higher difference between the two membrane layer areas than the smooth shape of roughly equal appearance, therefore the two shapes would be rather far apart in the phase diagram of the possible shapes. Shifting from one point to the other may involve processes required to overcome energy barrier(s) for example due to local bending energy of isotropic continuum [50]. Further, it is shown theoretically that the deviatoric effect is usually not uniformly distributed over the area of the vesicle so that in this respect the description by spontaneous warp (Eq.(79)) is oversimplified. Nevertheless, our results support the general ideas of deviatoric elasticity proposed by Fischer.

Some models of phospholipid bilayer membrane consider that the area per molecule may be different in the two membrane layers, but equal within each layer [64, 59]. This effect is referred to as the relative stretching of the two layers. Considering the relative stretching of the two layers, an additional nonlocal term appears in the expression for the bending energy of closed isotropic membrane bilayer [64, 59, 65]:

$$F_b = \frac{k_c}{2} \int (2H - \bar{C}_0)^2 dA + k_G \int C_1 C_2 dA + k_n A (\langle H \rangle)^2, \quad (80)$$

where

$$\langle H \rangle = \frac{1}{A} \int H dA, \quad (81)$$

is the average mean curvature and  $k_n$  is the nonlocal bending constant [64]. The effective spontaneous curvature of the bilayer  $\bar{C}_0$  [59, 66, 67] may derive from the bilayer asymmetry due to different environments on the two sides of the bilayer, due to their different compositions and due to different number of molecules in the two constituent monolayers [59, 64]. Eq.(80) can be rewritten in the equivalent form :

$$F_b = W_b + k_n A (\langle H \rangle - H_0)^2, \quad (82)$$

where  $W_b$  is given by Eq.(37) while the spontaneous average mean curvature  $H_0$  is proportional to the parameter  $\bar{C}_0$ . Using the relation between  $\Delta A$  and  $\langle H \rangle$  (Eqs.(60) and (81)) the energy  $F_b$  can be expressed also by the area difference  $\Delta A$  and the effective area difference  $\overline{\Delta A}_0 = 2A\delta H_0$  [65, 66, 67]. Now,  $\overline{\Delta A}_0$  and  $H_0$  depend on asymmetry in composition, environment and number of molecules between both monolayers. In accordance with the previous considerations [59, 66] it was established that these effects should not enter the expression for the bending energy of closed isotropic membrane bilayer (Eqs.(80) and(82)) independently but

only in the form of the (effective) spontaneous curvature of the bilayer  $\bar{C}_0$  or alternatively in the form of spontaneous average mean curvature  $H_0$  (or effective relaxed area difference  $\overline{\Delta A}_0$ ) [67]. However, in determining the equilibrium shape of the phospholipid vesicle with protrusion the estimated effect of the nonlocal bending (relative stretching of the two membrane layers) on the calculated stable shape was found to be negligible in the region of long thin protrusions [9].

If the tube radius were only several nanometers, the thickness of the membrane itself ( $\simeq 5\text{nm}$ ) is comparable to the radius of the protrusion. Therefore the expression for the area difference (Eq.(60)) should be restated [68] by considering that the membrane thickness is not very small comparing to the dimensions of the protrusion.

The crude model nevertheless shows that the deviatoric elasticity provides the explanation for the stability of the phospholipid nanotubes attached to the giant spherical phospholipid vesicles and for the observed shape transformation of the protrusion from the cylinder-like to the bead-like shape.

#### 4.4 Description of the collapse of inorganic nanotubes by deviatoric elasticity

We assume (similarly as in phospholipid nanotubes in the previous subsection) that the stable shape of the inorganic nanotube is determined by the minimum of the free energy of the nanotube wall; a variational problem is stated where it is required that the variation of the free energy with respect to the curvature field vanishes at given relevant constraints. For simplicity we consider a tube of a single S – Mo – S molecular layer. Also here we do not determine the rigorous solution of the variational problem; for description of the shape a parametrical model is used. Possible undulations of the tube are disregarded as we are focusing on the collapse of the tube where the cross section of the tube changes from a circle to a flattened shape while the cross section of the tube remains the same along the tube. It is assumed that the tube is very long so that the end effects can be neglected. The S – Mo – S layer is imagined to be divided into small patches so that the curvature of can be taken uniform over the patch. The patch is considered as the building unit. It is taken that the orientation of all the building units with respect to the geometrical axes of the tube are equal. The energy per area of a single unit is calculated by using Eq.(4),

$$\frac{dE}{dA} = \frac{\xi}{2}(H - H_m)^2 + \frac{\xi + \xi^*}{4}(\hat{C}^2 - 2\hat{C}\hat{C}_m \cos(2\omega) + \hat{C}_m^2). \quad (83)$$

It can be seen from Eq.(83) that the area density of the energy of the tube is characterized by two constants  $\xi$  and  $\xi^*$  and three parameters  $\omega$ ,  $H_m$  and  $\hat{C}_m$ .

We consider only the shapes with a constant cross-section along the longitudinal ( $\zeta$ ) axis. The cross-section of the tube lies in the  $(\chi, \psi)$  plane and is described by

the variational ansatz [46]

$$\psi(\chi) = \pm(a + \frac{(c\chi)^2}{1 + (c\chi)^2})\sqrt{b^2 - \chi^2}, \quad (84)$$

where  $a$ ,  $b$  and  $c$  are parameters and  $\chi \in [-b, +b]$ . The sign  $+$  pertains to the contour above the  $\chi$  axis and the sign  $-$  pertains to the contour below the  $\chi$  axis. By taking into account the definition of the principal curvatures [69],

$$C_1 = 0, \quad (85)$$

and

$$C_2 = -\frac{\psi''}{(1 + \psi'^2)^{3/2}}, \quad (86)$$

the mean curvature  $H$  and the curvature deviator  $D$  can be expressed as

$$H = -\frac{\psi''}{2(1 + \psi'^2)^{3/2}} \quad (87)$$

and

$$D = |H|, \quad (88)$$

where  $\psi' = d\psi/d\chi$  and  $\psi'' = d^2\psi/d\chi^2$ . The infinitesimal area element is

$$dA = \sqrt{1 + \psi'^2}d\chi d\zeta. \quad (89)$$

The mean curvature defined by Eq.(87) is positive for the convex regions (such as parts of sphere or cylinder) and automatically negative for the concave regions. The normal direction to the surface is outwards for all points. The curvature deviator (Eq.(88)) is always positive.

In the following, dimensionless quantities are used. The elastic energy of the tube is divided by  $\xi/2$  and calculated per unit of the normalized length  $L$  to yield a dimensionless quantity  $dE/d\zeta$  [46],

$$\frac{dE}{d\zeta} = \frac{2}{\xi L} \int \frac{dE}{dA} dA. \quad (90)$$

The minimum of the elastic energy is sought at constant dimensionless contour perimeter

$$2\pi \int \sqrt{1 + \psi'^2}d\chi = 2\pi R_0, \quad (91)$$

where  $R_0$  is the dimensionless radius of the cylindrical tube with the circular contour.

As the tube at the beginning grows into a cylindrical shape from a cylindrical shape of the S – Mo – S we start with the assumption that the initial equilibrium shape of the S – Mo – S layer is a cylinder ( $H_m = D_m > 0$ ) with certain orientation

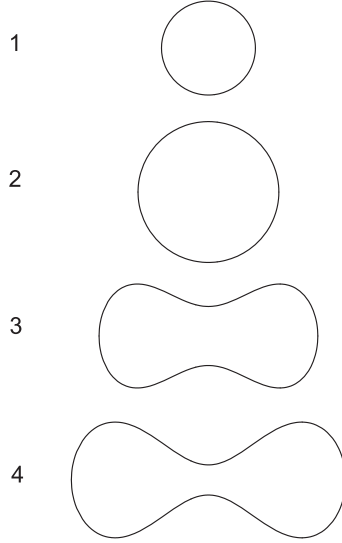


Figure 14: The calculated cross-sections of the equilibrium shapes of a single molecular layer for increasing relative perimeter of the tube;  $R_0$ : 1.0 (1), 1.5 (2), 2.0 (3) and 2.5 (4) at  $H_m = D_m = 1$  and  $\omega = 0$ . The cross-section of the tube is circular for  $R_0 < 1.87$  while the tube is in the collapsed state for larger  $R_0$  (from [46]).

of the atomic lattice with respect to the geometrical axes of the cylinder (for simplicity, it is taken that  $\omega = 0$ ). In the minimization of the free energy (Eq.(90)) the parameter  $c$  as the function of the parameters  $a$  and  $b$  is determined numerically from the constraint (91). The parameters  $a$  and  $b$  are then determined by the minimization of  $dE/d\zeta$ . The integrals in Eqs. (90) and (91) are calculated numerically. The material properties of the tube are described by the intrinsic mean curvature  $H_m$  and intrinsic curvature deviator  $D_m$ .

In general, for anisotropic thin closed plates (i.e. for  $D_m \neq 0$ ) the energy per unit of normalized length  $dE/d\zeta$  has two minima with respect to  $a$  and  $b$ . One minimum corresponds to the cylindrical tube with the circular contour, while the second minimum corresponds to the collapsed tube. At smaller values of  $R_0$  the minimum of  $dE/d\zeta$  corresponding to the cylindrical tube is the global minimum of  $dE/d\zeta$ . However, with increasing  $R_0$ , at a certain threshold, the minimum of  $dE/d\zeta$  corresponding to the collapsed tube, becomes the global minimum of  $dE/d\zeta$ .

Fig.14 shows the cross section of the calculated equilibrium shapes of the material with anisotropic properties ( $H_m = D_m = 1$ ). For simplicity, it is taken that  $\xi = \xi^*$ . The contour length  $R_0$  is increased from the top to the bottom. The tube cross-section is circular at smaller values of  $R_0$  while it is in the collapsed state above some threshold value of  $R_0$ . In contrast, for isotropic thin plates ( $D_m = 0$  and  $H_m \geq 0$ ) the calculated equilibrium state of the tube is cylindrical for all values of  $R_0$ . A nonzero

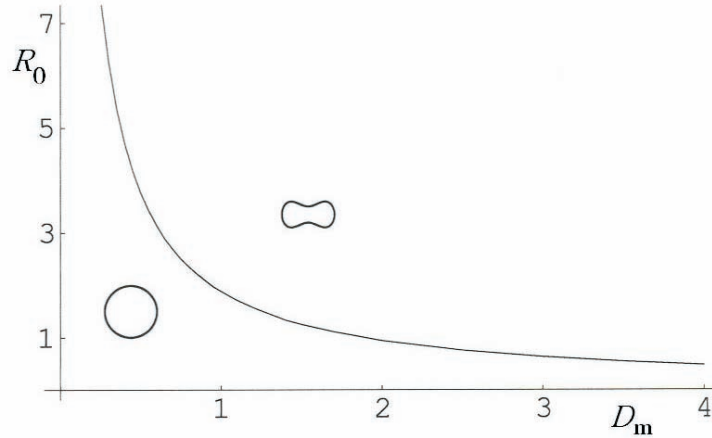


Figure 15: A  $(R_0, D_m)$  phase diagram of equilibrium shapes of the single-molecular-layer-tube with constant cross-section along the longitudinal axis;  $H_m = D_m$ ,  $\omega = 0$  (from [46]).

intrinsic curvature deviator is therefore prerequisite for the initiation of the collapse of the cylindrical tube with a large contour length. Based on these theoretical results we suggest that the observed collapse of the cylindrical MoS<sub>2</sub> micro and nanotubes that occurs during growth of the tube into a multilayer structure [23] is spontaneous, in order to keep the elastic energy of the tube as low as possible. Namely, during the growth of the tube into the multilayer structure the perimeter of the layers increases. For the outer layers the collapsed state becomes energetically more favorable. When this effect becomes large enough to render the collapsed state of the whole tube energetically the most favorable, the collapsed state becomes the stable state of the tube.

Fig.15 shows the  $(R_0, D_m)$  phase diagram exhibiting the regions corresponding to the stable shapes of the single-layer tube with constant closed cross-section along its longitudinal axis. The phase diagram shows two different regions of shapes: the region of cylindrical tubes with circular cross-section and the region of collapsed tubes. The critical value of  $R_0$  where the collapse of the tube occurs, decreases with increasing intrinsic curvature deviator  $D_m$  (Fig.15).

The collapsed shapes were observed also in carbon nanotubes [21]. It was suggested that the collapse of the carbon nanotube is initiated by some external mechanical force while the collapsed structure is kept stable by the van der Waals attractive forces between the nanotube walls [21]. The van der Waals forces are important also in stabilizing the collapsed shapes of MoS<sub>2</sub> micro and nanotubes, however, based on the presented results we argue that some other mechanism such as the intrinsic anisotropy of the molecular layer (described by the parameters  $H_m$  and  $D_m$ ) is necessary to trigger the collapse. The intrinsic anisotropy of the molec-

ular layer may be a consequence of the interaction between the layers. A perfect match of the two adjacent layers cannot be obtained, as the curvature of the adjacent layers is different. While in the direction of the tube axis the distance between the atoms may stay the same, the differences in the interatomic distances between individual layers are necessarily present along the tube circumference. In order to yield the most favorable match, defects in the structure may appear [18]. We may say that here the layer is described as a thin elastic plate with uniformly distributed anisotropic defects.

## **5 Deviatoric elasticity as a mechanism describing stable shapes of nanotubes**

The presented results show that the deviatoric elasticity deriving from orientational order of the building units of the system is a plausible mechanism that can explain some interesting features in hollow nanotubes. These features could not be explained by the standard continuum theory of elasticity where the material is treated as laterally isotropic. The basic assumption taken into account in the presented theory comprises the evident fact that the stable state of the nanotube is strongly anisotropically curved. Taken the tubular state as the state of the lowest energy for an individual building unit it is derived that the free energy of the system is conveniently expressed by two invariants of the curvature tensor: the mean curvature and the curvature deviator. The principle of deviatoric elasticity is useful in organic and in inorganic systems. To conclude, we propose that deviatoric elasticity should be taken into consideration as an essential feature in the systems of micro and nanometer scale.

## **6 Importance of the deviatoric effects in biology and technology**

### **6.1 The hypothesis of the subjacent membrane pool**

Within the fluid mosaic model of the structure of cell membranes [70] the membrane is described as a two dimensional liquid. Phospholipid bilayer forms a matrix while amphipathic proteins and/or oligosaccharides form inclusions that are embedded in the matrix. The inclusions may undergo translational diffusion within the membrane and normally have no long-range order [70]. It was suggested [70] that the general principles of the fluid mosaic model apply to most biological membranes such as plasmalemmal and intracellular membranes, including the membranes of different cellular organelles, such as mitochondria and chloroplasts (thereby called functional membranes). It was also suggested that there existed some membranous systems such as myelin or lipoprotein membranes of small animal viruses that may be rigid

and have different properties than the functional membranes. These latter systems were considered rather as special cases.

Thirty years of experimental evidence strongly supports the general features of the fluid mosaic model referring to functional membranes. However, as we have argued in this contribution, it is indicated that the behavior of the cellular membranes in highly anisotropically curved regions may deviate from the behavior of two dimensional liquid and rather exhibits properties of a two dimensional liquid crystal with in-plane orientational order of the membrane constituents [51, 50, 13].

Membrane constituents are in general nonaxisymmetric with respect to the axis pointing in the direction normal to the membrane. The energy states of these molecules therefore depends on the in-plane orientation of the molecule and an orientation exists that is the most favorable for such molecule. In almost flat regions the effect of the orientational ordering of the membrane constituents is negligible, however, it may become important in highly anisotropically curved regions such as in cylindrical and toroidal regions pertaining to the blebs [12, 71] or toroidal regions pertaining to the edge of the pores [72] thereby stabilizing these structures. Adding detergent dodecylmaltoside to the suspension of erythrocytes causes the erythrocyte membrane to develop spicules (Fig.16). Thin tubular protrusions are formed on top of the spicules (Fig.16) [12]. These protrusions grow in length and are eventually detached from the cell (Fig.1) probably due to external forces that are acting in the solution.

As the wrinkling of the membrane and formation of the vesicles and pores are common processes in cells, the highly anisotropic structures that are not directly visible may be commonly present in cells. A possibility exists that the pool of the membrane material in this state is rather large and that it forms the infrastructure for the processes taking place in the cell interior as well as for the communication with the cell exterior. We call the pool of the membraneous material present in highly anisotropic curved structures the subjacent pool of the membraneous material. For clarity, we call the membraneous material in almost flat regions the superficial pool. We propose a hypothesis that the presence and state of the subjacent pool of the membraneous material is a general feature in cells. This hypothesis is essentially a refinement of the fluid mosaic model of the membrane structure, however, we believe that this refinement may provide an insight into vitally important phenomena that generally take place in cells.

One such phenomenon is directed transport of membrane vesicles in cellular processes. Transport vesicles play a central role in the traffic of molecules between various membrane-enclosed compartments of cellular secretory pathways and in the transport of materials taken up at the cell surface [73].

Recently, it was observed that the transport vesicles (blebs) may travel along the tube attached to the giant phospholipid vesicle while the existence of small blebs of membrane micro and nanotubes was also observed in red blood cells [75]. Based on these results it can be anticipated that micro and nanotube directed transport of

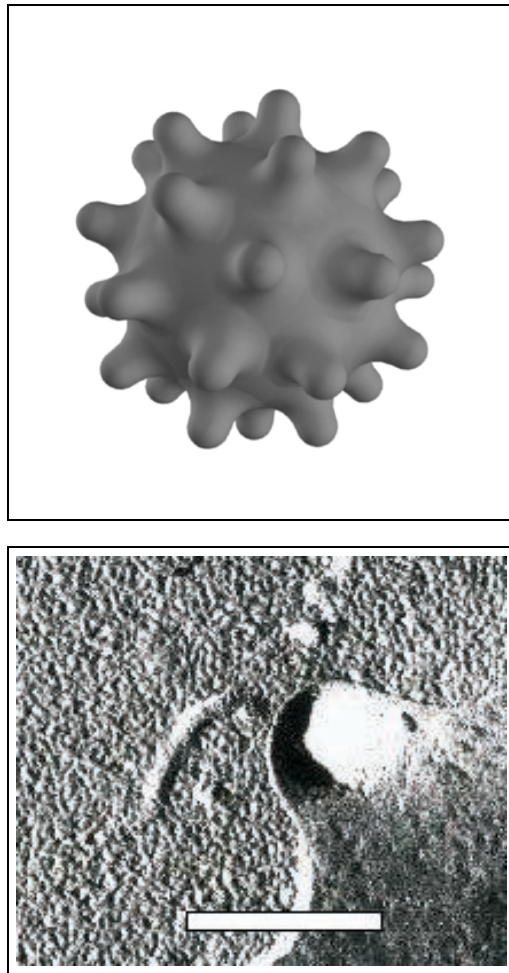


Figure 16: Upper picture: a scheme of the spiculated erythrocyte (echinocyte). Lower picture: a scanning electron micrograph of the replica of the erythrocyte membrane following the freeze fracture method [32]; the echinocytosis and development of tubular buds on top of echinocyte spicules was induced by incubating erythrocyte suspension with detergent dodecylmaltoside [74]. The cells were fixed and freeze-fractured. The freeze-fracture replicas were examined by a Cambridge Instrument S360 microscope [32]. Bar = 500nm.

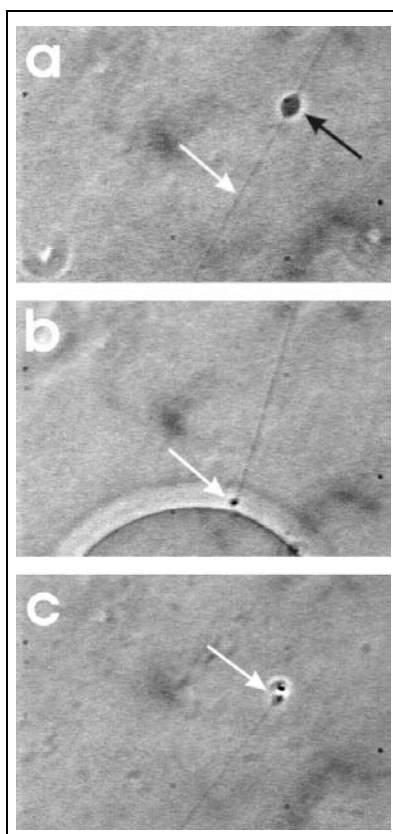


Figure 17: A bleb (black arrow) of phospholipid tube (white arrow) (a) that acts as a transport vesicle for the enclosed material. One end the phospholipid tube is attached to the bilayer membrane (b), while the other end of the tube is attached to the glass surface of the observation chamber (c). The vesicles were observed under the inverted microscope Zeiss IM 35 with the phase contrast optics (from [75]).

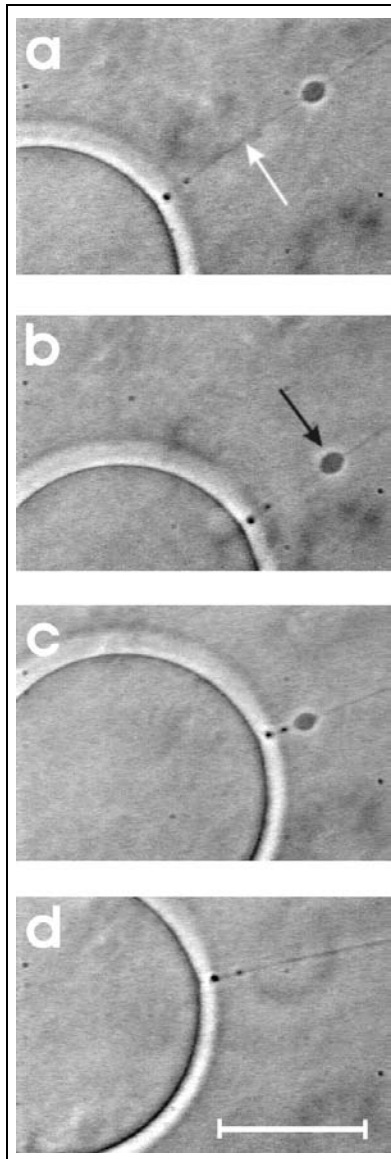


Figure 18: Transport of a small phospholipid prolate bleb (black arrow) along a thin phospholipid tube (white arrow). Note that the bleb (transport vesicle) is an integral part of the tube membrane. Scale bar,  $10\mu\text{m}$ . The vesicles were observed under the inverted microscope Zeiss IM 35 with the phase contrast optics (from [75]).

vesicles could have an important role in the selectivity of specific pathways of transport vesicles in cellular systems where the transport vesicles must move specifically from one membrane enclosed compartment to another compartment. The transport to the target point would be much more efficient if the nanotubes directed the vesicles. We would like to point to this possibility.

As the nanotubes may be very thin the connected vesicles may seem as diffusing freely in the solution. It was observed in erythrocytes that the daughter vesicles may be connected by nanotubes to the parent cell [13]. The nanotubes could not be directly observed, however the vesicles moved synchronously with the mother cell indicating their connection with the parent cell by nanotubes [13].

In observing a sample of POPC vesicles that were prepared as described in the subsection “Preparation of phospholipid vesicles connected by nanotubes” an interesting phenomenon was observed [75]: a giant spherical vesicle was attached to the glass by a long thin tether. On the tether, a small bleb slowly moving towards the mother sphere was observed. Fig.17a shows a bleb (black arrow) of the phospholipid tube. One end of the tube is attached to the bilayer membrane of the giant POPC vesicle (Fig. 17b) while the other end of the nanotube is attached to the glass surface of the observation chamber (Fig.17c). The length of the tube is several diameters of the mother vesicle.

Fig.18 shows transport of a small prolate bleb (black arrow) along the thin phospholipid tube. In the beginning the bleb was far away from the surface of the giant phospholipid vesicle (Fig. 18a). The bleb moved continuously towards the surface of the giant phospholipid vesicle (Figs.18a, b, c). In the vicinity of the surface of the giant liposome the bleb started to oscillate slightly back and forth along the tube. Also, the shape and size of the bleb changed, i.e. the bleb became elongated and appeared to lose volume. In the final stage the contents of the bleb fused with the giant liposome (Fig.18d).

We cannot say how the observed bleb of the phospholipid membrane was produced, however, a following time course was speculated [75]: when after the electroformation the vesicles were rinsed into the observation chamber, a configuration where two vesicles were connected by a thin tether was produced. One of the vesicles was large, the other was small. The small vesicle may have attached to some defect (Fig.17c) in the glass. There is always slight convective current in the observation chamber. This current caused the excess pressure on both vesicles. The movement of the larger vesicle caused the nanotube to straighten while the excess pressure on the small vesicle pushed it along the nanotube. The small vesicle started moving and became a bleb (Fig.17a). The bleb was followed from the moment it was spotted to the integration with the larger vesicle (Fig.18d) for about half an hour [75]. The observation started about an hour after the process of electroformation was completed and the vesicles were rinsed out from the electroformation chamber. When spotted, the bleb was about halfway between the origin of the tube on the glass and the insertion of the tube on the larger vesicle. It was moving slowly towards the

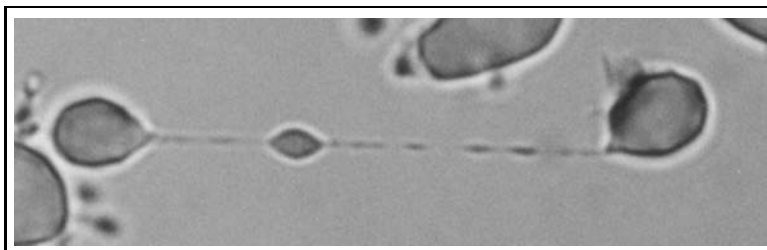


Figure 19: A micrograph showing a small prolate vesicle of a red blood cell membrane tube connecting the two membrane-enclosed parts of a disintegrated red blood cell. The red blood cells were observed in isotonic physiological solution with added dibucaine at  $\text{pH} \approx 8.5$ . Scale bar,  $3\mu\text{m}$  (from [75]).

larger vesicle retaining its shape and size throughout. When the bleb reached the larger vesicle (Fig.18c), the current pressure eventually pushed its contents through the neck connecting the bleb and the larger vesicle.

There are related phenomena where beads corresponding to transient excited states were produced by a sudden tension in the membrane tubes that is induced either by laser tweezers [76] or by mechanical manipulation [77] (see also [78]). No such procedure was involved in the above experiment. The vesicles produced by electroformation pertain to quasi-equilibrium states and not to transient excited states. The blebs (transport vesicles) are regarded as stable. On the other hand, excited states of the membrane [76] are relaxed after a certain time (depending on the shape of the blebs; slight undulations are relaxed in seconds while sphere-like blebs connected by thin tubular parts are relaxed in minutes [76]).

Small blebs (vesicles) of thin membrane tubes were also observed in red blood cells [75]. The erythrocyte suspension was pipetted into an Eppendorf tube containing a high pH buffer. Incubation of the red blood cells at high pH resulted first in an echinocytic shape transformation (development of spicules) and microvesiculation. As incubation continued, large spherical daughter vesicles were shed from the cell surface. The release of the rather large vesicles was accelerated by addition of dibucaine. The erythrocytes were observed by optical microscope with phase contrast optics. Fig.19 shows a small prolate bleb of the thin membrane tube connecting two membrane-enclosed parts of the red blood cell into which the cell disintegrated under the described external conditions. The bleb was observed for about half an hour during which it more or less retained its size and shape.

The observed blebs (Figs.17)-(19) are large regarding intracellular mechanisms, however, the same mechanism of the transport by blebs should be relevant also for smaller blebs, provided that they are made stable. In the intracellular transport the shape of transport vesicles may be additionally stabilized by mechanisms that are not present in the simple system of one-component phospholipid vesicles, as for example by clathrin coating [79] or other protein and lipid domain formation

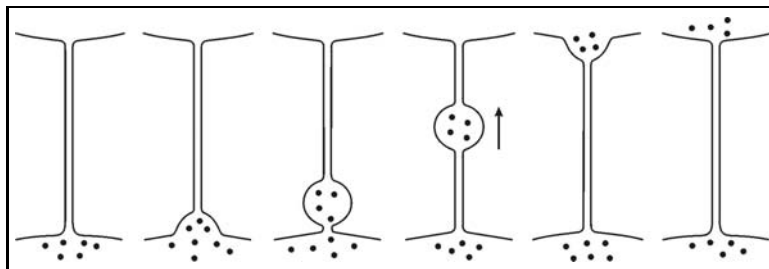


Figure 20: Schematic presentation of a possible mechanism of micro and nanotube directed traffic of transport vesicles between two membrane-enclosed compartments (from [75]).

mechanism [80, 81]. In the transport, the contents of the nanotube and of the bleb are expected to mix, however, if the nanotube is very thin, it could not contain much volume.

Since the nanotubes are difficult to visualize and are also very fragile, the proposed mechanism of directed vesicle transport may have been overlooked in biological systems, though it could have an important role in the function of the Golgi system and other cellular transport systems involving vesicles.

## 6.2 Aspects of possible applications of MoS<sub>2</sub> nanotubes

Due to their cylindrical geometry, these novel advanced nano-materials have a low mass density, a high porosity and an extremely large surface to weight ratio. Their potential applications range from high porous catalytic and ultralight anticorrosive materials, atomic probes and electron field emitters to non-toxic strengthening fibers. This may lead to a more efficient use and an increase in durability of materials. Doping of these semiconducting nano-structured materials may also allow further miniaturization of electronic systems and may lead to new optoelectronic materials. The helical structure of undoped tubes with semiconductor behaviour and their optical activity enable possible applications in nonlinear optics and in solar cell technology. By functionalizing the nanotubes, e.g. using specific Mo containing enzymes, novel functional biomaterials could be made. Using capilar forces the MoS<sub>2</sub> nanotubes could be used as nanopipes or at storage containers for biomaterials.

## References

- [1] J.M. Schnur, *Science* **262**, 1669 (1985).
- [2] S. Chiruvolu, H.E. Warriner, E. Naranjo, K. Kraisler, S.H.J. Idziak, J. Radler, R.J. Plano, J.A. Zasadzinsky and C.R. Safinya, *Science* **266**, 1222 (1994).
- [3] D. Težak, S. Punčec and M. Martins, *Liq. Cryst.* **23**, 17 (1997).

- [4] N. Shahidzadeh, D. Bonn, O. Aguerre-Chariol and J. Meunier, *Phys. Rev. Lett.* **81**, 4268 (1998).
- [5] N. Shahidzadeh, D. Bonn, O. Aguerre-Chariol and J. Meunier, *Colloids Surf. A* **147**, 375 (1999).
- [6] R. Oda, I. Huc, M. Schmutz, S.J. Candau and F.C. MacKintosh, *Nature* **399**, 566 (1999).
- [7] L. Mathivet, S. Cribier and P.F. Devaux, *Biophys. J.* **70**, 1112 (1996).
- [8] V. Kralj-Iglič, G. Gomišček, J. Majhenc, V. Arrigler and S. Svetina, *Colloids Surf. A* **181**, 315 (2001).
- [9] V. Kralj-Iglič, A. Iglič, G. Gomišček, F. Sevšek, V. Arrigler and H. Hägerstrand, *J. Phys. A: Math.Gen.* **35** 1533 (2002).
- [10] H.U. Lutz, A.J. Lomant, P. McMillan and E. Wehrli, *J. Cell Biol.* **74**, 389 (1977).
- [11] W.T. Coakley, A.J. Bater and J.O.T. Deley, *Biochim. Biophys. Acta* **512**, 318 (1978).
- [12] V. Kralj-Iglič, A. Iglič, H. Hägerstrand and P. Peterlin, *Phys. Rev. E* **61**, 4230 (2000).
- [13] V. Kralj-Iglič, A. Iglič, H. Hägerstrand and M. Bobrowska - Hägerstrand, *Colloids Surf. A* **179**, 57 (2001).
- [14] S. Ochs, R. Pourmand, R.A. Jersild Jr. and R.N. Friedman, *Progress in Neurobiology* **52**, 391 (1997).
- [15] V. Kralj-Iglič, U. Batista, H. Hägerstrand, A. Iglič, J. Majhenc and M. Sok, *Radiol. Oncol.* **32**, 119 (1998).
- [16] U. Gimsa, V. Kralj-Iglič, A. Iglič, J. Gimsa, *Songklanakarín J. Sci. Tehcnol.*, in print.
- [17] S. Iijima, *Nature* 354 (1991) 56.
- [18] D.J. Srolovitz, S.A. Safran, M. Homyonfer and R. Tenne, *Phys. Rev. Lett.* **74**, 1779 (1995).
- [19] B.I. Yakobson, C.J. Brabec and J. Bernholc, *Phys. Rev. Lett.* **76**, 2511 (1996).
- [20] W. Marx, M. Wanitschek and H. Schier, *Condensed Matter News* **7**, 3 (1999).
- [21] N.G. Chopra, R.J. Luyken, K. Cherrey, V.H. Crespi, M.L. Cohen, S.G. Louie and A. Zettl, *Science* **269**, 966 (1995).

- [22] A.M. Rao, E. Richter, S. Bandow, B. Chase, P.C. Eklund, K.A. Williams, S. Fang, K.R. Subbaswamy, M. Menon, A. Thess, R.E. Smalley, G. Dresselhaus and M.S. Dresselhaus, *Science* **275**, 187 (1997).
- [23] M. Remškar, Z. Škraba, M. Regula, C. Ballif, R. Sanjines and F. Levy, *Adv. Mater.* **10**, 2 (1998).
- [24] M. Remškar, Z. Škraba, F. Cleton, R. Sanjines and F. Levy, *Surf. Rev. Lett.* **5**, 423 (1998).
- [25] S.J. Tans, R.M. Verschueren and C. Dekker, *Nature* **393**, 49 (1998).
- [26] M. Remškar, A. Mrzel, Z. Škraba, A. Jesih, M. Čeh, J. Demšar, P. Stadelmann, F. Levy, D. Mihailovič, *Science* **292**, 479 (2001).
- [27] H. Nakamura and Y. Matsui, *J. Am. Chem. Soc.* **117**, 2651 (1995).
- [28] P. Hoyer, *Langmuir* **12**, 141 (1996).
- [29] W.Q. Han, S.S. Fan, Q.Q. Li and Y.D. Hu, *Science* **277**, 1287 (1997).
- [30] L. Guo, Z. Wu, T. Liu, W. Wang and H. Zhu, *Chem. Phys. Lett.* **318**, 49 (2000).
- [31] G. Seifert, H. Terrones, M. Terrones and T. Frauenheim, *Solid State Communications*, **15**, 635 (2000).
- [32] H. Hägerstrand, unpublished.
- [33] M. Remškar, unpublished.
- [34] G. Cevc and D. Marsh, *Phospholipid bilayers*, (Wiley - Interscience, New York, 1987).
- [35] *Handbook of Nonmedical Applications of Liposomes*, D.D. Lasic and Y. Barenholz, eds., (CRC Press, Boca Raton, 1996).
- [36] H.T. Tien, A. Ottova, in: H.T. Tien and A. Ottova-Leitmannova, eds., *Planar Lipid Bilayers (BLMs) and Their Applications*, Elsevier, Amsterdam, London, 2003, 1-74.
- [37] M. Remškar, Z. Škraba, C. Ballif, R. Sanjines, F. Levy, *Surf. Sci.* **637**, 433 (1999).
- [38] M. Remškar, Z. Škraba, F. Cleton, R. Sanjines, F. Levy, *Appl. Phys. Lett.* **69** 351 (1996).
- [39] M. Remškar, Z. Škraba, R. Sanjines, F. Levy, *Appl. Phys. Lett.* **74** 3633 (1999).

- [40] M.I. Angelova, S. Soleau, Ph. Meleard, J.F. Faucon and P. Bothorel, *Prog. Colloid Polym. Sci.* **89**, 127 (1992).
- [41] V. Heinrich, R.E. Waugh, *Ann. Biomed. Eng.*, **24** 595 (1996).
- [42] J.V. Selinger, F.C. MacKintosh and J.M. Schnur, *Phys. Rev. E* **53**, 3804 (1996).
- [43] R. Tenne, L. Margulis, M. Genut, and G. Hodes, *Nature* **360** 444 (1992).
- [44] M. Nath, A. Govindaray, C.N.R. Rao, *Adv. Mater.* **13** 283 (2001).
- [45] C.M. Zelenski, P.K. Dorhout, *J. Am. Chem. Soc.*, **120** 734 (1998).
- [46] V. Kralj-Iglič, M. Remškar, G. Vidmar, M. Fošnarič and A. Iglič, *Phys. Lett. A* **296** (2002) 151.
- [47] L.D. Landau, E.M. Lifshitz, *Theory of Elasticity*, (Reed Educational and Professional Publishing Ltd., 1986).
- [48] G. Gouy, *J. Phys. France* **9**, 457 (1910).
- [49] D.L. Chapman, *Philos. Mag.* **25** 475 (1913).
- [50] V. Kralj-Iglič, V. Heinrich, S. Svetina and B. Žekš, *Eur. Phys. J. B* **10** 5 (1999).
- [51] J.B. Fournier, *Phys. Rev. Lett.* **76** 4436 (1996).
- [52] A. Iglič, V. Kralj-Iglič, B. Božič, M. Bobrowska - Hägerstrand and H. Hägerstrand, *Bioelectrochemistry* **52** 203 (2000).
- [53] H. J. Deuling, W. Helfrich, *J. Phys. France* **37** 1335 (1976).
- [54] W. Helfrich, *Z. Naturforsch.* **28c** 693 (1973).
- [55] H.P. Duwe, J. Käs, E. Sackmann, *J. Phys. (France)* **51** 945 (1990).
- [56] U. Seifert, *Adv. Phys.* **46** 13 (1997).
- [57] M.P. Sheetz and S.J. Singer, *Proc. Natl. Acad. Sci. USA* **72** 4457 (1974).
- [58] E.A. Evans, *Biophys. J.* **14** 923 (1974).
- [59] W. Helfrich, *Z. Naturforsch.* **29c** 510 (1974).
- [60] S. Svetina, A. Ottova-Leitmannova, R. Glaser, *J. Theor. Biol.* **94** 13 (1982).
- [61] J. Käs and E. Sackmann, *Biophys. J.* **60**, 825 (1991).
- [62] T. Fischer, *J. Phys. II (France)* **2** 337 (1992).
- [63] T. Fischer, *J. Phys. II (France)* **3** 1795 (1993).

- [64] E.A. Evans, R. Skalak, *Mechanics and Thermodynamics of Biomembranes*, (CRC Press Inc., Boca Raton, 1978).
- [65] B.T. Stokke, A. Mikkelsen, A. Elgsaeter, *Eur. Biophys. J.* **13** 203 (1986).
- [66] L. Miao, U. Seifert, M. Wortis and H.G. Döbereiner, *Phys. Rev. E* **49** 5389 (1994).
- [67] R. Mukhopadhyay, G. Lim, M. Wortis, *Biophys. J.* **82** 1756 (2002).
- [68] I. Szleifer, D. Kramer, A. Ben-Shaul, W.M. Gelbart and S.A. Safran, *J. Chem. Phys.* **92** 6800 (1990).
- [69] M. Vygodsky, *Mathematical Handbook - Higher Mathematics* (Mir Publishers, Moscow, 1975).
- [70] S.J. Singer and G.L. Nicholson, *Science*, **175** 720 (1972).
- [71] M. Bobrowska - Hägerstrand, V. Kralj - Iglič, A. Iglič, K. Bialkowska, B. Isomaa and H. Hägerstrand, *Biophys. J.* **77**, 3356 (1999).
- [72] M. Kandušer, M. Fošnarič, M. Šentjurs, V. Kralj-Iglič, H. Hägerstrand, A. Iglič, D. Miklavčič, *Colloids Surf. A* **214** 205 (2003).
- [73] G. M. Cooper, *The Cell, a Molecular Approach*, (ASM Press, Sunderland, 2000).
- [74] H. Hägerstrand and B. Isomaa, *Biochim. Biophys. Acta* **1109** (1992) 117.
- [75] A. Iglič, H. Hägerstrand, M. Bobrowska-Hägerstrand, V. Arrigler, V. Kralj-Iglič, *Phys. Lett. A* **310** 493 (2003).
- [76] R. Bar-Ziv and E. Moses, *Phys. Rev. Lett.* **73** 1392 (1994).
- [77] E. Evans, W. Rawicz, *Phys. Rev. Lett.* **64** 2094 (1990).
- [78] R. E. Goldstein, P. Nelson, T. Powers, U. Seifert, *J. Phys. II (France)* **6** 767 (1996).
- [79] W. Stoorvogel, V. Oorschot and H.J. Geuze, *J. Cell. Biol.* **132** 21 (1996).
- [80] C. Thiele, M.J. Hannah, F. Fahrenholz and B. Huttner, *Nature Cell. Biol.* **2** 42 (2000).
- [81] J.M. Holopainen, M.I. Angelova and K.J. Kinnunen, *Biophys. J.* **78** 830 (2000).